POLITECNICO DI TORINO

UNIVERSITÉ PARIS SUD

Master degree course in Physics of Complex Systems

Master Degree Thesis

Deformation of glassy states in p-spin models

Supervisors:
Dr. Pierfrancesco Urbani
Prof. Andrea Pagnani

Candidates
Jack Thomas Parley
matricola: 24524

Anno accademico 2017-2018

Summary

In this master's thesis we consider the p-spin spin glass model, in both its spherical and Ising versions, as a schematic model for amorphous solids. In the first part of the thesis, we briefly review the main properties of the spherical p-spin model, focusing in particular on the free energy landscape and the metastable/glassy states. We then introduce a model for studying the deformation of these glassy states, consisting in the addition of an s-spin term to the original p-spin Hamiltonian. This $p + \epsilon s$ deformation is then studied by considering the Franz-Parisi potential, which allows us to follow the glassy states and study their stability under the external perturbation.

Considering first the spherical p-spin, a rich phase diagram is found by varying the degree of annealing (T_g) and the value of s. Fixing $p = 3$, we find that for small s ($s < 3$) the glass yields in a replica-symmetric, elastic regime. However when s is increased to higher values, the glass may undergo a Gardner transition to marginal stability before yielding. The same analysis is carried out in the Ising p-spin, where we also find RS-stable yielding for $s = 2$, and a Gardner transition for higher values of s ($s \geq 3$). Monte carlo simulations, employing the planting technique, are performed to test some of the predictions in the elastic case.

Finally, we consider how the formalism may be extended in order to characterise the fluctuations at the yielding point; this may be approached analytically in the spherical p-spin, while improved simulation techniques may be employed in the Ising p-spin in order to study the statistics of avalanches.

Acknowledgements

I would like to thank the Istitut de Physique Théorique (IPhT), CEA Saclay, where this master's thesis work was carried out.

Contents

Chapter 1

Introduction

In this introduction we will first briefly discuss some of the main aspects of the physics of glasses, which are the physical objects under study in this work. We will then discuss (also briefly) some of the main aspects of the behaviour of glasses under strain (their rheology), which present us with the interesting physical phenomena which we are attempting to elucidate in this work using simple mean-field spin glasses.

1.1 Glasses and the Random First Order Transition Theory

A glass, or amorphous solid, may be simply defined as a solid with no crystalline order. What makes it a *solid*, is that it is capable of responding elastically to an externally applied shear derformation. However, a glass or amorphous solid is fundamentally different from its crystalline counterpart; instead of being organized in a regular lattice, the elementary degrees of freedom are positioned at random in space, and there is no underlying order.

The glass phase is exhibited by members of all liquid types, including molecular, ionic and metallic liquids. These glass forming liquids, instead of crystallizing upon cooling, can be supercooled below the melting temperature T_m and then solidify at some temperature T_g, the *glass transition temperature* [1]. Understanding from a theoretical viewpoint both the glass phase and the related glass transition pose a great challenge. Indeed, what are the mechanisms that drive the freezing of the supercooled liquid into the glass? Unlike for other well-understood phase transitions, one cannot reason along the lines of symmetry breaking, given that the glass phase is apparently just as disordered or amorphous as the supercooled

liquid one.

Here we will restrict ourselves to one of the many theories proposed to understand this phenomenon, namely the *Random First Order Transition Theory* (RFOT) [2]. The reason for this is the deep relation between this theory and the physics of the mean-field spin glasses considered in this work (see part I). On the other hand, structural glass models (e.g. hard spheres), which may be solved exactly in the limit of infinite dimension, realize precisely the scenario emerging from the RFOT.

The RFOT affords us with a picture of the glass transition from the point of view of the underlying phase space. According to this picture, sufficiently deep in the supercooled region, the phase space gets clustered into a large number of metastable states, which are what we refer to as glasses. In *finite dimension*, these glassy states or amorphous structures have a finite (albeit very long) lifetime. The relaxational dynamics in the supercooled phase can be thought of as a set of jumps from one state to the other. The jumps are well separated in time, and between them the system explores ergodically the current metastable state. When the system is cooled even further, the lifetime of the metastable states increases in an exponential way with temperature, until at the so-called Kauzmann temperature (T_K) there is an ideal thermodynamic transition where this lifetime diverges.

In this work we will remain always in mean field (infinite dimension), and therefore the glassy states will have an infinite lifetime. This presents us with a great advantage: these glassy states may be studied with purely static tools. This is the approach we will take in this work, following glassy states under external perturbations as in [3][4][5]. Instead of considering structural glasses, however, we will consider much simpler models, namely the p-spin (spherical and Ising) mean-field spin glass models. Despite their simplicity, these models reproduce some of the main behaviour of glasses, while being fully solvable from the analytical point of view.

1.2 Glasses under deformation

Understanding the complex response of glassy/amorphous solids to deformations is a central problem in condensed matter. Besides the fundamental interest in finding a unified microscopic point of view [6], the problem also has important consequences in material design and applications.

This problem has been approached in many different ways, but here we will be most interested in the behaviour of the simplest model of an amorphous solid,

namely dense assemblies of hard spheres [7]. The main reason for this is that the mean-field HS (hard sphere) model has been solved exactly in infinite dimensions, and thus the phase diagram can be studied analytically [8]. Among other aspects, these results have particularly shed light on one of the crucial properties of the response of amorphous solids, namely the *stability*, i.e. on how a glass may become unstable due to increased plasticity under shear deformations.

In [7], extensive numerical simulations are used in order to map out exhaustively the behaviour of HS spheres under normal and shear stress. We here focus on the typical stress-strain behaviour of an HS glass (see figures in [7]) obtained through simulations, which seems to follow the general predictions of the mean-field theory in $d \to \infty$ [4]. Starting from equilibrated configurations at some value of the packing fraction $\varphi_g > \varphi_d$, the quasi-static evolution of the system is followed under the shear strain γ. The system is sheared up to a maximum value, and then sheared back in the reversed way [1]. One may identify three regimes of the stress-strain curve, which corrrespond to stable, marginally stable, and unstable states:

1. **The elastic regime**, where the stress σ increases smoothly and monotonically with increasing γ. To first order, the response is linear, $\delta\sigma = \mu\delta\gamma$, μ being the shear modulus. Once the strain is reversed, the stress-strain curve reverses to the origin, thus consituting an *elastic* response.

2. **The marginally stable/plastic regime**. Above a certain threshold γ_G, the stress-strain curve becomes jerky, consisting of piecewise linear elastic responses followed by small and abrupt stress drops, which correspond to plastic events. The system is *marginally stable*, and thus a tiny increment $\delta\gamma$ can cause these avalanches; but the particles can find immediately another stable configuration and the material therefore resists entire failure. In this regime the system is partially irreversible: for small reversed strain the stress-strain curve is locally irreversible, but globally it may be reversed back to the origin.

3. **Yielding**[2]. At the yielding strain γ_Y, a sudden and significant stress drop takes place. Once the glass breaks (yields), the system is irreversible. In particular, if one measures the relative mean square displacement Δ_r between the initial and final configurations, this becomes non-zero in the irreversible

[1] In [7] the cyclic deformation actually comprises also a change in the normal stress, leading also to possibe shear jamming (instead of shear yielding), but we will omit this here.

[2] We omit the possibility of shear jamming, considered also in [7]

case (in the reversible case $\Delta_r = 0$, meaning that the initial and final configurations are identical).

In terms of the free energy landscape, the glass corresponds to a basin, which becomes distorted under increasing strain. In the infinite-dimensional solution, we may identify the first regime with the RS (replica symmetric)-stable phase, while γ_G corresponds to a Gardner transition to marginal stability (the basin becomes rough). In this marginally stable state, the system can release the stress via hopping between different sub-basins, corresponding to plastic events. Finally at *yielding* the system escapes the basin, corresponding to a *spinodal point* in the infinite-dimensional solution.

The main purpose of this work is to study these effects in the spherical and Ising p-spin spin glass models, which although much simpler than hard spheres, show some of the key aspects of glassy behaviour (see part I). Instead of considering the mean square displacement Δ_r between particle configurations (see [7]), we will consider the relative overlap between spin configurations q_r; instead of a shear we will consider an s-spin deformation. Despite these differences, we will see that these simple models show intriguing similarities with amorphous solids.

Part I

Physics of the p-spin

Chapter 2

Spherical p-spin model

In this chapter we first define the model and review some of the main concepts for studying spin glasses. We then discuss the free-energy landscape of the spherical p-spin model, focusing in particular on the complexity and the metastable states in the glassy region. Finally these same results are explained from a different perspective by considering the Franz-Parisi potential, which will in turn constitute the basis of the state following approach developed in part II.

2.1 Definition and basic concepts

The p-spin model was first introduced in its Ising version in [9] and [10], and the spherical counterpart was introduced later in [11]. The p-spin Hamiltonian is defined as:

$$H_p[\underline{\sigma}, J] = -\sum_{i_1<\cdots<i_p} J_{i_1\ldots i_p}\sigma_{i_1}\cdots\sigma_{i_p} \qquad p \geq 3 \tag{2.1}$$

In the spherical version of the model, the spins σ_i are real continous variables which are constrained to live on the surface of a sphere of radius $\sqrt{N}$, that is $\sum_{i=1}^{N}\sigma_i^2 = N$. What makes the model a spin glass is the quenched disorder in the couplings, which are Gaussian random variables with zero mean and variance given by:

$$\overline{J^2_{i_1\cdots i_p}} = \frac{p!}{2N^{p-1}} \tag{2.2}$$

where the overbar denotes average over the quenched disorder. The variance is chosen in this manner to ensure the proper scaling of the free energy and energy

with system size.

Self-averaging and the replica method

When dealing with spin glasses, an important concept is that of self-averaging. The problem is that in principle, the observables (including the free energy), will depend on the specific realization of the disorder J [1], and will thus obviously vary from sample to sample. Luckily, for large enough systems, the free energy density will no longer depend on the couplings J, and will converge to a J-independent value given by:

$$F = -\lim_{N\to\infty} \frac{1}{\beta N} \overline{\log Z(J)} = F_\infty(\beta) \tag{2.3}$$

Calculating the quenched average $\overline{\log Z}$ is very difficult. This is where the replica trick comes into play. It stems from the following simple mathematical expressions for writing a logarithm:

$$\overline{\log Z} = \lim_{n\to 0} \frac{1}{n} \log \overline{Z^n} = \lim_{n\to 0} \frac{\overline{Z^n} - 1}{n} = \lim_{n\to 0} \partial_n \overline{Z^n} \tag{2.4}$$

If n remains a real number, there is no advantage in doing this. However, if we can promote n to an integer, we can write:

$$\overline{Z^n} = \int \mathrm{D}\sigma^{(1)} \dots \mathrm{D}\sigma^{(n)} \exp\left(\overline{-\beta H[\sigma^{(1)}, J] \cdots - \beta H[\sigma^{(n)}, J]}\right) \tag{2.5}$$

which is easier to compute.

In fact, it will become even more problematic, as in order to do the calculations we will exchange the $n \to 0$ and thermodynamic limits:

$$F = -\frac{1}{\beta} \lim_{n\to 0} \lim_{N\to\infty} \frac{1}{N} \partial_n \overline{Z^n} \tag{2.6}$$

We will come back to this point in the following chapter.

Pure states

In the low temperature phase, and in the thermodynamic limit $N \to \infty$, it is well known that some systems may present ergodicity breaking: the system at

[1] Here J is used to denote all the couplings.

equilibrium only explores a sub-part of the phase space. In this situation one may split the Gibbs measure into sub-components called *pure states*:

$$\langle\cdot\rangle = \sum_{\alpha} w_\alpha \langle\cdot\rangle \tag{2.7}$$

where α runs over all the states, and their relative weights are defined as:

$$w_\alpha = \frac{Z_\alpha}{Z} \tag{2.8}$$

Z_α being the partition function restricted to state α.

An important feature of pure states is the *clustering* property. This states that the statistical correlation between two points goes to zero when their distance goes to infinity:

$$\langle\sigma_i\sigma_j\rangle \to \langle\sigma_i\rangle\langle\sigma_j\rangle \quad \text{for} \quad |i-j|\to\infty \tag{2.9}$$

Using this property, we may show for example that the paramagnetic state (that is the Gibbs ergodic measure over the full phase space) in the Ising model below T_c is not a pure state. We have

$$\langle\sigma_i\sigma_j\rangle = \frac{1}{2}\langle\sigma_i\sigma_j\rangle_+ + \frac{1}{2}\langle\sigma_i\sigma_j\rangle_- \tag{2.10}$$

where we have split the measure into two states with positive (+) and negative (-) spontaneous magnetization. As $|i-j|\to\infty$:

$$\langle\sigma_i\sigma_j\rangle \to \frac{1}{2}\langle\sigma^2\rangle_+ + \frac{1}{2}\langle\sigma^2\rangle_- = m^2 \neq 0 \tag{2.11}$$

In the case of the Ising model, we have simply two states which are characterized by a uniform magnetization. In a disordered system in the mean field limit, for a given sample (realization of the J's) each state is characterized by an amorphous magnetization profile. The TAP (Thouless Anderson Palmer) [12] free energy $F[m]$ will thus posess many local minima, which we will call TAP states (they are solutions of the TAP equations, i.e. minima of the TAP free energy functional) [13] [14].

2.2 The static and dynamical transitions

In this section we will discuss the most important aspects of the model, focusing on the structure of the pure states.

The states of the spherical p-spin model are sketched in figure 2.1 [2]. A key aspect of the spherical p-spin model is that the spin glass states at zero temperature, labelled by their intensive energy e at zero temperature, maintain their identity and can be followed in their evolution at $T > 0$ [13]. At zero temperature, the number of states of energy e is $\Omega(e) = \exp\left(N\Sigma_0(e)\right)$, where we have defined the *complexity* function $\Sigma_0(e)$. $\Sigma_0(e)$ is a concave function that vanishes at e_{min} and goes to zero discontinously at some threshold value e_{th}. Likewise, at higher temperatures $T > 0$, one may define

$$\Omega(f) = \sum_{\alpha} \delta\left(f - f_\alpha\right) = \exp\left(N\Sigma(f)\right) \tag{2.12}$$

where $\sum_\alpha$ denotes a sum over pure states, and $\Sigma(f) = \Sigma_0(e(f))$, $e(f)$ being the $T = 0$ energy of the states of free energy f. Like its zero-temperature counterpart, $\Sigma(f)$ vanishes continously at f_{min} and drops to zero above f_{th}.

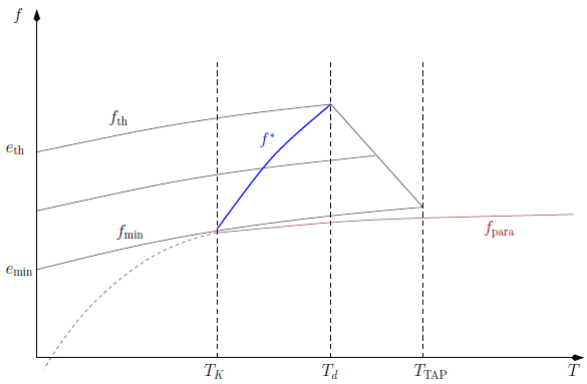

Figure 2.1: Evolution in temperature of the p-spin states, reproduced from [14].

We may now write the full partition function Z in terms of pure states. Indeed, one can think of $Z_\alpha = \exp\left(-\beta N f_\alpha\right)$ as the contribution of this state to the total partition function. One has:

[2] Note that $\frac{\mathrm{d}f}{\mathrm{d}T} = -s$, and so in the case of the spherical p-spin the free energy increases in temperature because the entropy is negative (the variables are continous). For discrete variables (such as Ising p-spin) the reverse is true.

$$Z = \exp\left(-\beta N f_{tot}(T)\right) \sim \sum_{\alpha} \exp\left(-\beta N f_{\alpha}\right) =$$
$$\int \mathrm{d}f \sum_{\alpha} \delta\left(f - f_{\alpha}\right) \exp\left(-\beta N f_{\alpha}\right) = \int \mathrm{d}f \Omega(f) \exp\left(-\beta N f\right) =$$
$$\int_{f_{min}}^{f_{th}} \mathrm{d}f \exp\left(N\left[\Sigma(f) - \beta f\right]\right) \sim \exp\left(N\left[\Sigma(f^*) - \beta f^*\right]\right) \quad (2.13)$$

where $f^* \in [f_{min}, f_{th}]$ is such that $f - T\Sigma(f)$ is minimum, i.e.

$$\left.\frac{\mathrm{d}\Sigma}{\mathrm{d}f}\right|_{f^*} = \frac{1}{T} \quad (2.14)$$

Starting from high temperature, one encounters three distinct temperature regions. These are separated by a dynamical transition temperature T_d, and a static transition temperature T_K [3].

- $T > T_d$

  Above T_d, the phase space is ergodic and the system is in the paramagnetic (liquid) state. The free energy is given by $f_{para}(T)$.

- $T_K < T < T_d$

  At the dynamical transition T_d, the phase space gets clustered into an exponential (in the system size) number of metastable states. Because of the mean-field nature of the model, energy barriers are infinite, and therefore if the system is prepared in one of these states it remains trapped there forever [4]. Importantly, this phenomenon can only be seen from studying the dynamics. The reason for this is the equality $f^*(T) - T\Sigma f^*(T) = f_{para}(T)$ (where $f_{para}(T)$ is just the extrapolation to low temperature of the free energy of the paramagnet) in the whole interval $T \in [T_K, T_d]$.

[3] The letter K in T_K stands for Kauzmann, since it coincides with the Kauzmann temperature in structural glasses.

[4] If we allow for timescales exponentially large in N, the system can escape a glassy state.

- $T < T_K$

  At T_K, there is a thermodynamic phase transition; the free energy and its first derivatives are continuous, but the second derivative of $f_{tot}(T)$ with respect to T (the specific heat) has a jump. Below T_K, the phase space is dominated by the lowest free energy states, $f_{tot}(T) = f_{min}(T)$.

In the range of temperature $T_K < T < T_d$, one can decompose the entropy into two contributions:

$$s(T) = \Sigma(T) + s_{vib}(T) \tag{2.15}$$

where $\Sigma(T) = \Sigma(f^*(T))$ is the configurational entropy of the states that dominate the partition function at temperature T, and $s_{vib}(T)$ is the internal (*vibrational*) entropy within these states. This scenario realizes the so-called Random first order transition (RFOT) theory [2]. At $T = T_K$, $\Sigma(T)$ vanishes (the so-called *entropy crisis*) and we get a jump in the specific heat as the system freezes into the lowest-lying states.

2.3 The Franz-Parisi potential method

We will now present a different way of studying the physics in the interval $T_K < T < T_d$ [3], which is of particular interest due to its connection with the state following formalism developed in the following sections.

The starting point is to consider a reference configuration $\sigma^{(1)}$, and then the partition function of a replica $\sigma^{(2)}$ which has an additional term in the Hamiltonian coupling it to configuration $\sigma^{(1)}$[5]:

$$Z\left(\sigma^{(1)}, \epsilon, T\right) = \int \mathrm{D}\sigma^{(2)} \exp\left(-\beta H_p\left[\sigma^{(2)}\right] + \beta N \epsilon q_{\sigma^{(1)},\sigma^{(2)}}\right) \tag{2.16}$$

where the function $q_{a,b}$ gives the overlap between two configurations a and b. We have:

$$q_{\sigma^{(1)},\sigma^{(2)}} = \frac{1}{N}\sum_{i=1}^{N} \sigma_i^{(1)}\sigma_i^{(2)} \tag{2.17}$$

[5]We will omit the overbar, that is the partition functions and free energies are averaged over the disorder (J-independent).

The free energy associated to 2.16 depends on $\sigma^{(1)}$, but if $\sigma^{(1)}$ is extracted at equilibrium at temperature T this dependence should disappear (in the thermodynamic limit). Thus one may average over the equilibrium distribution of $\sigma^{(1)}$ at T to obtain

$$F(\epsilon, T) = -\frac{1}{\beta N} \int \mathrm{D}\sigma^{(1)} \frac{\exp\left(-\beta H_p\left[\sigma^{(1)}\right]\right)}{Z(\beta)} \log\left(Z\left(\sigma^{(1)}, \epsilon, T\right)\right) \tag{2.18}$$

Interested in the behaviour for vanishing coupling strength ϵ, we now introduce the Franz-Parisi potential [3] $V(q_r, T)$ as

$$V(q_r, T) = \max_{\epsilon} \left[F(\epsilon, T) + \epsilon q_r\right] \tag{2.19}$$

where the conjugate variable to the coupling field ϵ is given by (q_r stands for relative overlap):

$$q_r(\epsilon) = -\frac{\partial F(\epsilon, T)}{\partial \epsilon} = \left\langle q_{\sigma^{(1)}, \sigma^{(2)}} \right\rangle_{\epsilon} \tag{2.20}$$

The Franz-Parisi [3] potential $V(q_r, T)$ is then the free energy of the system $\sigma^{(2)}$ constrained to be at a fixed overlap q_r with $\sigma^{(1)}$:

$$V(q_r, T) = -\frac{1}{\beta N} \int \mathrm{D}\sigma^{(1)} \frac{\exp\left(-\beta H_p\left[\sigma^{(1)}\right]\right)}{Z(\beta)} \log\left(Z\left(\sigma^{(1)}, q_r, T\right)\right) \tag{2.21}$$

$$Z\left(\sigma^{(1)}, q_r, T\right) = \int \mathrm{D}\sigma^{(2)} \exp\left(-\beta H_p\left[\sigma^{(2)}\right]\right) \delta\left(q_r - q_{\sigma^{(1)}, \sigma^{(2)}}\right) \tag{2.22}$$

Physically, what the Legendre transform is telling us is that $\frac{\mathrm{d}V}{\mathrm{d}q_r} = \epsilon(q_r)$, and therefore the possible average values of the order parameter (the relative overlap) are given by $\frac{\mathrm{d}V}{\mathrm{d}q_r} = 0$, the *minima* of the FP potential.

The FP potential $V(q_r, T)$ is plotted for different temperatures in figure 2.2. At high temperature ($T > T_d$), the function has a single minimum at $q_r = 0$, as there is only a paramagnetic phase where the two copies $\sigma^{(1)}$ and $\sigma^{(2)}$ are uncorrelated.

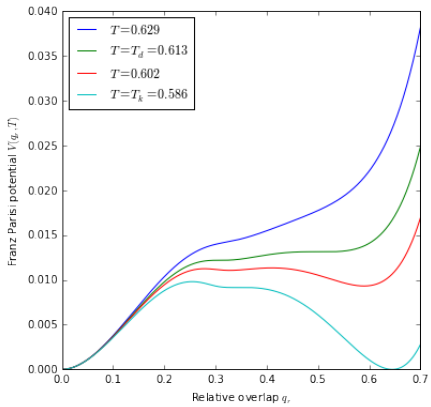

Figure 2.2: The Franz Parisi potential for different temperatures, spherical p-spin (p=3)

At T_d, there is an inflection point and a secondary minimum appears at $q_r^{min}(T)$, corresponding to the self-overlap of the equilibrium TAP states at temperature T. However, this minimum is *metastable*, as the probability of finding the two copies in the same TAP state (at zero coupling) is vanishing due to the complexity (the number of states is exponential in N).

At $T = T_K$, $V(q_r^{min}(T_K), T_K)$ becomes equal to $V(0, T_K)$. In fact, all this can be seen quantitatively by realizing that $V(q_r^{min}(T), T)$ is the free energy of the equilibrium TAP states, and $V(0, T)$ is just the paramagnetic free energy $f_{tot}(T)$. One then has:

$$V(q_r^{min}(T), T) - V(0, T) = f^*(T) - f_{para}(T) = T\Sigma(f^*(T)) \tag{2.23}$$

And thus the difference in free energy vanishes at T_K, where the complexity vanishes $\Sigma(f^*(T_K)) = 0$. We have therefore recovered the physics of the previous section from a new viewpoint.

Part II

Deforming p-spin glassy states

Chapter 3

Introduction

Before turning to the original part of this work, we will first briefly discuss the main results of the work by Berthier, Barrat and Kurchan [15], where the driven dynamics of the p-spin was considered as a model for the non-linear rheology of glassy materials. We will then present the model considered in this work, highlighting the differences and similarities with respect to [15].

3.1 Driven dynamics for non-linear rheology

In [15], the dynamics of the p-spin under a non-conservative driving force were studied. The relaxational (non-driven) Langevin dynamics in the spherical p-spin model is just given by:

$$\dot{\sigma}_j(t) = -\mu(t)\sigma_j(t) - \frac{\partial H_p[\sigma]}{\partial \sigma_j(t)} + \eta_j(t) + h_j(t) \tag{3.1}$$

where $\eta_j(t)$ is a Gaussian white noise, with $\langle \eta_j(t) \rangle = 0$ and $\langle \eta_j(t)\eta_l(t') \rangle = 2T\delta_{jl}\delta\left(t - t'\right)$. $\mu(t)$ is a Lagrange multiplier which is introduced in order to enforce the spherical constraint $\frac{1}{N}\sum_j^N \sigma_j^2(t) = 1$, and $h_j(t)$ is an external field which for now will only be used to evaluate the linear response. When studying the dynamics, one is mostly interested in the correlation function $C(t,t')$ and the linear response function $R(t,t')$, defined by:

$$C(t,t') = \frac{1}{N}\sum_j \langle \sigma_j(t)\sigma_j(t') \rangle \qquad R(t,t') = \frac{1}{N}\sum_j \left.\frac{\delta \langle \sigma_j(t) \rangle}{\delta h_j(t')}\right|_{h=0} \tag{3.2}$$

We will not consider here the full derivation (which can be found for example in [13]) , but using the generating functional approach one may average over the

disorder, and finally obtain *effective* equations for a *single* degree of freedom which moves in an environment which must be determined self-consistently.

The main results regarding the relaxational dynamics (no drive) are as follows. Above the dynamical temperature $T > T_d$, it is possible to find a stationary solution ($C(t,t') = C(t-t')$ and $R(t,t') = R(t-t')$), where the correlation and response functions are related through the fluctuation-dissipation theorem. As one approaches T_d, the relaxation splits into a fast timescale where the correlation descends to a plateau $q_d < 1$, and then a slow timescale (associated to collective rearrangements) on a scale τ_α which diverges at T_d. Below T_d, on the other hand, the system can no longer equilibrate. One may still define a stationary ("fast") regime down to a plateau $q_{th} > q_d$, but the "slow" relaxation becomes non stationary. In particular, if one looks at $C(t,t')$ as a function of $\tau = t - t'$ for fixed t', it decays to zero for $\tau >> \tau_\alpha(t')$, where $\tau_\alpha(t')$ is an increasing function of t' (*aging*) that diverges for $t' \to \infty$. In terms of the free energy landscape, what happens in the aging regime is that the system gets stuck in increasingly long-lived traps just above the threshold f_{th}.

In [15], the authors introduce an external driving force, which is non-conservative (cannot be written as deriving from a potential):

$$h_j(t) = \frac{\epsilon}{(k-1)!} \sum_{j,j_1\dots,j_{k-1}} \widetilde{J}_{j,j_1\dots j_k} \sigma_{j_1} \cdots \sigma_{j_{k-1}} \tag{3.3}$$

where the $\widetilde{J}_{j,j_1\dots,j_{k-1}}$ are independent random Gaussian couplings, also independent from the ones of the Hamiltonian, and have variance $\frac{k!}{2N^{k-1}}$. These couplings are *not* symmetric in the exchange $j \leftrightarrow j_l$, although they are still symmetric in the exchange of two indices j_l.

The main results the authors obtain are as follows [15]. On the one hand, the α-relaxation time t_α (the slow timescale associated to collective rearrangements) is studied as a function of the driving ϵ, for temperatures above and below T_d. At zero driving ($\epsilon = 0$), it is known that t_α increases as T_d is approached from above, until it diverges at T_d, and for temperatures below T_d indeed one has $\lim_{\epsilon\to 0} \tau_\alpha(\epsilon, T) = \infty$. The effect of the driving is that the system becomes stationary for all temperature and driving forces; it reaches a *non-equilibrium steady-state*. Indeed in the $T < T_d$ regime, the drive continuously injects energy into the system and allows it to explore freely the landscape without getting trapped.

On the other hand, the authors also consider the consequences for *rheology* [15]. Given that the injected power is given by $\frac{\epsilon^2}{t_\alpha}$, one may also associate $\frac{\epsilon}{t_\alpha}$ to a shear rate ($\dot\gamma$) and ϵ to a stress (σ). The main effects are *shear thinning* both above and

below T_d, and for $T < T_d$ the appearance of a yield stress, that is $\sigma(\dot{\gamma} \to 0) \neq 0$. A finite driving force (power injection) is needed to keep the system at the threshold where it may flow freely.

Moreover, in [16] the analysis was extended to the case where the system is prepared in one of the deep regions below the threshold. From the topology of the free energy landscape, one expects that a weak driving force will have no effect beyond a trivial 'elastic' response, as it is not enough to allow the system to overcome the barriers. Instead a strong driving force lets the system escape from the state and surf on the threshold, and then keeps it there forever. These expectations are confirmed by the calculations performed in [16], where the existence of a *static yield stress* $\sigma_Y(T)$ is proved, beyond which the system shows liquid behaviour in its non-equilibrium steady state.

3.2 Our model

In the present work we will not study the dynamics, but instead consider a *constrained* thermodynamics, applying the methods first developed in [3] to study glassy states. Starting from an equilibrium glass of the p-spin selected at a temperature $T_g \in [T_K, T_d]$, we follow this state under the addition of a perturbation in the form of an s-spin Hamiltonian, that is:

$$\begin{aligned} H_p[\underline{\sigma}] &\to H_p[\underline{\sigma}] + \epsilon H_s[\underline{\sigma}] \\ &= -\sum_{i_1<\cdots<i_p} J_{i_1\ldots i_p}\sigma_{i_1}\cdots\sigma_{i_p} - \epsilon \sum_{i_1<\cdots<i_s} \widetilde{J}_{i_1\ldots i_s}\sigma_{i_1}\cdots\sigma_{i_s} \end{aligned} \tag{3.4}$$

where the *deforming* couplings are extracted from an independent Gaussian distribution, with zero mean and variance given by $\overline{\widetilde{J}^2_{i_1\cdots i_s}} = \frac{s!}{2N^{s-1}}$.

When the glass is thus followed under the perturbation, it may be deformed up to a spinodal point ϵ_Y, which we identify as the *yielding* point. This is a purely conservative deformation, and all the analysis is restricted to the state being deformed.

Intuitively, one may expect that as high values of s are considered, the glass basin may become more and more rugged and develop a compex hierarchical structure of sub-basins before it reaches yielding. Indeed, if one considers the *pure* s-spin free energy landscape, for higher values of s the number of states increases, their volume shrinks and the barriers between them are higher [17]. The possible replica symmetry breaking before yielding will be studied by the *replicon* eigenvalue, while the mode that becomes unstable at the spinodal point is the so-called *longitudinal*

mode.

We do not, however, consider the full statics or free energy landscape of the mixed model defined by $p+\epsilon s$, as done in [18] or [19]. We are instead simply following a p-spin equilibrium glass as the overall landscape evolves adiabatically towards that of a mixed model. Moreover, we do not consider at any point the final stationary state once the glass yields. One may say that at the spinodal the system becomes unstable against ergodization; the order parameter (the relative overlap) jumps from the original high value to a lower value, signaling that the system has exited the now unstable glass basin. However, whether the new phase which appears at the spinodal is the paramagnetic (liquid) phase of the mixed model, or whether the system instead surfaces on the threshold, or eventually falls into another deep state, are issues which we cannot address in this purely static approach.

Chapter 4

Deforming spherical p-spin glassy states

In this chapter we study the evolution of spherical p-spin glassy states under a deformation of the form $\epsilon H_s[\underline{\sigma}]$. The calculation of the Franz-Parisi potential in the RS ansatz is first presented, and then its stability is studied by the replicon mode. An extensive numerical study of the equations is then performed to characterize the different behaviours at different values of s and T_g (the glass preparation temperature).

4.1 *Reference* and *constrained* replicas

In order to study a glassy state under perturbation, we will proceed in a similar spirit as in section 2.3, where the so-called *potential method* was described. The main difference will be that the *constrained* replica $\sigma^{(2)}$ will now have an additional term in its Hamiltonian, namely an s-spin perturbation term[1].

We are interested in calculating the free energy of the glass under the ϵ-deformation, i.e. the potential:

$$V_{FP}(q_r) = -\frac{1}{\beta N}\overline{\int \mathrm{D}\sigma^{(1)}\, \frac{\exp\left(-\beta H_{\epsilon=0}[\sigma^{(1)}]\right)}{Z_{\epsilon=0}} \log\left(Z_\epsilon\left(\sigma^{(1)}, q_r\right)\right)}^{(J_p, \widetilde{J}_s)} \tag{4.1}$$

[1]The ϵ strength of the perturbation is not to be confused with the coupling ϵ in the potential method.

where $Z_\epsilon\left(\sigma^{(1)}, q_r\right)$ is the partition function of a *constrained* replica, which is under a Hamiltonian $H_p + \epsilon H_s$ and has fixed overlap q_r with $\sigma^{(1)}$:

$$Z_\epsilon\left(\sigma^{(1)}, q_r\right) = \int \mathrm{D}\sigma^{(2)} \exp\left(-\beta\left(H_p\left[\sigma^{(2)}\right] + \epsilon H_s\left[\sigma^{(2)}\right]\right)\right)\delta\left(q_r - q_{\sigma^{(1)},\sigma^{(2)}}\right) \tag{4.2}$$

As explained in section 2.3, once we average over the equilibrium ensemble of $\sigma^{(1)}$, we lose the dependence on the reference configuration, and we obtain the partition function of the glass we are following under the deformation. It will be useful to denote this average over the reference configuration by brackets, to distinguish it from the one over the couplings (denoted by the overbar):

$$\left\langle \cdot \right\rangle = \int \mathrm{D}\sigma^{(1)} \frac{\exp\left(-\beta H_{\epsilon=0}[\sigma^{(1)}]\right)}{Z_{\epsilon=0}} \cdot \tag{4.3}$$

With this notation the Franz-Parisi potential (4.1) is just:

$$V_{FP}(q_r) = -\frac{1}{\beta N}\overline{\left\langle \log\left(Z_\epsilon\left(\sigma^{(1)}, q_r\right)\right)\right\rangle}^{(J_p,\widetilde{J}_s)} \tag{4.4}$$

Making use of the replica trick, one may also write equation (4.1) as:

$$V_{FP}(q_r) = -\frac{1}{\beta N}\lim_{m\to 0}\lim_{n\to 0}\partial_n \overline{\int \mathrm{D}\sigma^{(1)} \exp\left(-\beta H_{\epsilon=0}[\sigma^{(1)}]\right) Z_{\epsilon=0}^{m-1} Z_\epsilon^n\left(\sigma^{(1)}, q_r\right)}^{(J_p,\widetilde{J}_s)} \tag{4.5}$$

We have thus introduced not one but n constrained replicas, which will allow us to probe possible replica symmetry breaking in the glass. The number of reference replicas has also been upgraded to m, and the n constrained replicas are restricted to having a fixed relative overlap q_r with the first of the reference ones. One must therefore compute the following replicated partition function:

$$Z^{(m,n)} = \int \mathrm{D}\sigma^{(1)} \exp\left(-\beta H_{\epsilon=0}[\sigma^{(1)}]\right) Z_{\epsilon=0}^{m-1} Z_\epsilon^n(\sigma^{(1)}, q_r) \tag{4.6}$$

and take the appropriate limits.

4.2 The replicated partition function

If may make explicit the integration, expression 4.6 becomes:

$$Z^{(m,n)} = \int \mathrm{D}\sigma^{(a)} \int \mathrm{D}\sigma^{(\alpha)} \overline{\exp\left(-\beta \sum_{a=1}^{m} H_p[\sigma^{(a)}] - \beta \sum_{m+1}^{m+n} \left(H_p[\sigma^{(\alpha)}] + \epsilon H_s[\sigma^{(\alpha)}]\right)\right)}^{(J_p,\widetilde{J}_s)} \prod_{\alpha=m+1}^{m+n} \delta\left(q_{\sigma^{(1)},\sigma^{(\alpha)}} - q_r\right) \quad (4.7)$$

where the index $a = 1, .., m$ runs over the m *reference* replicas and the index $\alpha = m+1, ..., n$ over the n *constrained* ones. The first step is to average over the disorder (the couplings):

$$\overline{\exp\left(\beta\left(\sum_{a=1}^{m} H_p[\sigma^{(a)}] + \sum_{\alpha=m+1}^{m+n} H_p[\sigma^{(\alpha)}] + \epsilon \sum_{\alpha=m+1}^{m+n} H_s[\sigma^{(\alpha)}]\right)\right)}^{(J_p,\widetilde{J}_s)} \quad (4.8)$$

Giving the terms

$$\prod_{i_1<\cdots<i_p} \int \mathrm{d}J_{i_1\cdots i_p} \exp\left(-J^2_{i_1\cdots i_p} \frac{N^{p-1}}{p!} + J_{i_1\cdots i_p}\beta\left(\sum_{a=1}^{m} \sigma^{(a)}_{i_1}\cdots\sigma^{a}_{i_p} + \sum_{\alpha=m+1}^{m+n} \sigma^{(\alpha)}_{i_1}\cdots\sigma^{(\alpha)}_{i_p}\right)\right) \quad (4.9)$$

and

$$\prod_{i_1<\cdots<i_s} \int \mathrm{d}\tilde{J}_{i_1\cdots i_s} \exp\left(-\tilde{J}^2_{i_1\cdots i_s} \frac{N^{s-1}}{s!} + \beta\epsilon\tilde{J}_{i_1\cdots i_s} \sum_{\alpha=m+1}^{n+m} \sigma^{\alpha}_{i_1}\cdots\sigma^{\alpha}_{i_s}\right) \quad (4.10)$$

These are simple Gaussian integrals.

Ignoring pre-factors and using that $p!\sum_{i_1<\cdots<i_p} \sim \sum_{i_1,\cdots,i_p}$ for large N, we find an expression where the sites are now uncoupled; the replicas are instead, through their overlaps. The overlaps can be simply expressed in matrix form, by defining:

$$\mathbf{Q}_{ab} = \frac{1}{N}\sum_{i=1}^{N} \sigma^a_i \sigma^b_i \qquad a, b = 1, \ldots m+n \quad (4.11)$$

This $(m+n)\times(m+n)$ $\mathbf{Q}$ matrix can be split into three submatrices Q, R and P.

$$\mathbf{Q} = \begin{bmatrix} Q & P \\ P^T & R \end{bmatrix} \tag{4.12}$$

where Q is an $m \times m$ matrix containing the overlaps between the m reference replicas, R is $n \times n$ and contains the overlaps of the n constrained replicas, and P is an $m \times n$ matrix with the overlaps between each of the m reference replicas and the n constrained ones.

The above Gaussian integrals yield:

$$\exp\left(\frac{N\beta^2}{4}\left(\sum_{a,b=1}^{m} Q_{ab}^p + \sum_{\alpha,\beta=m+1}^{m+n} R_{\alpha\beta}^p + 2\sum_{a=1}^{m}\sum_{\alpha=m+1}^{m+n} P_{a\alpha}^p + \epsilon^2 \sum_{\alpha,\beta=m+1}^{m+n} R_{\alpha\beta}^s\right)\right) \tag{4.13}$$

Besides this we must evaluate the jacobian $J(\mathbf{Q})$, resulting from the transformation from integrating over the spins to integrating over the overlaps. That is

$$J(\mathbf{Q}) = \int \mathrm{D}\sigma^{(a)} \prod_{a\leq b} \delta\left(N\mathbf{Q}_{ab} - \sum_i \sigma_i^a \sigma_i^b\right) \tag{4.14}$$

This can be shown to give a contribution $\frac{1}{2}\mathrm{Tr}\,(\log \mathbf{Q})$ [13], which can be expressed in terms of the submatrices Q, P and R by using the following property:

$$\mathrm{Tr}\,(\log \mathbf{Q}) = \mathrm{Tr}\,(\log Q) + \mathrm{Tr}\left(\log\left(R - P^T Q^{-1} P\right)\right) \tag{4.15}$$

The integral can finally be written in the form:

$$Z^{(m,n)} \propto \int \mathrm{d}\mathbf{Q} \exp N S(\mathbf{Q}) \tag{4.16}$$

And one can evaluate it in the $N \to \infty$ limit by taking the saddle point. We must therefore find Q, P, R which extremize

$$S(Q,P,R) = \frac{\beta^2}{4}\left(\sum_{a=1}^{m}\sum_{b=1}^{m} Q_{ab}^p + \sum_{\alpha=1}^{n}\sum_{\beta=1}^{n} R_{\alpha\beta}^p + 2\sum_{a=1}^{m}\sum_{\alpha=1}^{n} P_{a\alpha}^p + \epsilon^2 \sum_{\alpha=1}^{n}\sum_{\beta=1}^{n} R_{\alpha\beta}^s\right) + \frac{1}{2}\mathrm{Tr}\,(\log Q) + \frac{1}{2}\mathrm{Tr}\left(\log\left(R - P^T Q^{-1} P\right)\right) \tag{4.17}$$

4.3 Replica symmetric equations

To begin with, we must consider the parametrization of the matrices Q, P and R. We consider the m reference replicas to be in the high-temperature phase, and take a replica-symmetric ansatz $Q_{ab} = \delta_{ab}$, where the 1 on the diagonal is due to the spherical constraint and the replicas have zero overlap among each other. Strictly speaking, in the interval $T_K < T < T_d$ the phase space is not ergodic, but because there is an exponential number of states the probability distribution of the overlap is trivial $\overline{P(q)} = \delta(q)$ [3]. On the other hand, P will just be parametrized by q_r, which measures the relative overlap with the reference replica. Therefore we have:

$$Q = \delta_{ab} \qquad P_{a\alpha} = \delta_{a,1} q_r \tag{4.18}$$

For the matrix R we will at first take a replica symmetric ansatz parametrized by q, that is $R_{\alpha\beta} = \delta_{\alpha\beta} + (1 - \delta_{\alpha\beta})q$. Importantly, the previous ansatz for Q and P will remain unchanged even when replica symmetry breaking (RSB) is considered for R, given that the reference system is completely independent from the constrained one.

Using these ansatz, the expression for the action S becomes:

$$\begin{aligned} S^{(m,n)}(Q,P,R) &= \frac{\beta^2}{4}\left[m + n(1+\epsilon^2) + n(n-1)(q^p + \epsilon^2 q^s) + 2nq_r^p\right] \\ &+ \frac{1}{2}\left[n\log\left(1-q_r^2\right) + (n-1)\log\left(\frac{1-q}{1-q_r^2}\right) + \log\left(1 + (n-1)\frac{q-q_r^2}{1-q_r^2}\right)\right] \end{aligned} \tag{4.19}$$

We now take the appopiate limits to find the Franz-Parisi potential V_{FP}, given by[2]:

$$\begin{aligned} V_{FP} &= -\frac{1}{\beta}\lim_{m\to 0}\lim_{n\to 0}\frac{\partial}{\partial n} S^{(m,n)}(q, q_r, q_g) \\ &= -\frac{1}{2\beta}\left\{-\frac{\beta^2}{2}\left(q^p + \epsilon^2 q^s\right) + \beta^2 q_r^p + \frac{\beta^2}{2}(1+\epsilon^2) + \log(1-q) + \frac{q-q_r^2}{1-q}\right\} \end{aligned} \tag{4.20}$$

[2] In [3], the authors substract the equilibrium free energy and consider $V_{FP} - f(T)$; they therefore do not have the term $-\frac{\beta}{4}$ (paramagnetic free energy) in the final expression of the potential.

We now look for the saddle point equations for q and q_r. Deriving with respect to q and q_r we find

$$-2\beta\frac{\partial V_{FP}}{\partial q} = \frac{q-q_r^2}{(1-q)^2} - \frac{\beta^2}{2}\left(pq^{p-1} + \epsilon^2 sq^{s-1}\right) = 0 \tag{4.21}$$

$$-2\beta\frac{\partial V_{FP}}{\partial q_r} = \beta^2 pq_r^{p-1} - 2\frac{q_r}{1-q} = 0 \tag{4.22}$$

Note that at $\epsilon = 0$, if we look for a solution with $q_r = q$ we find that both parameters obey the same equation, namely

$$\frac{\beta^2}{2}pq^{p-1} = \frac{q}{1-q} \qquad \frac{\beta^2}{2}pq_r^{p-1} = \frac{q_r}{1-q_r} \tag{4.23}$$

This equation has only the trivial solution $q_r = q = 0$ at high temperatures, but if we lower the temperature there appears a non-trivial solution $q_r = q > 0$ at the so-called dynamical transition temperature T_d.

Choosing $T_K \leq T \leq T_d$, our starting point will thus be $\epsilon = 0, q_r = q > 0$. Once we apply a deformation ($\epsilon \neq 0$) we will need to find q and q_r by solving equations (4.21) and (4.22) self-consistently. We may write equations (4.21) and (4.22) in the following form:

$$q_r = \frac{\beta^2}{2}pq_r^{p-1}(1-q) \equiv f(q_r, q) \tag{4.24}$$

$$q = q_r^2 + (1-q)^2\frac{\beta^2}{2}\left[pq^{p-1} + \epsilon^2 sq^{s-1}\right] \equiv g(q_r, q) \tag{4.25}$$

which will be more convenient.

4.3.1 Internal energy

We may also compute the internal energy of the glass in the replica symmetric phase. Here we need to be careful to distinguish the reference and constrained replicas. Indeed, to reach expression (4.20) we have considered that both the *reference* and the *slave* replicas are at the same inverse temperature β. In the original work by Franz and Parisi [3], the reference replicas are at equilibrium at β' and the constrained replicas are instead at an inverse temperature β which can be varied. The corresponding potential is then:

$$V_{FP}(q_r, \beta, \beta') = -\frac{1}{\beta N}\overline{\left\langle \log\left(Z_\epsilon\left(\sigma^{(1)}, q_r\right)\right)\right\rangle}^{(J_p, \widetilde{J}_s)} \tag{4.26}$$

where now the reference configuration is at an inverse temperature β', so the average $\langle\cdot\rangle$ is in this case:

$$\left\langle \cdot \right\rangle = \int \mathrm{D}\sigma^{(1)} \frac{\exp\left(-\beta' H_{\epsilon=0}[\sigma^{(1)}]\right)}{Z_{\epsilon=0}(\beta')}. \tag{4.27}$$

Proceeding in the same way as shown previously, one has that this more general potential is given by [3]:

$$V_{FP}(q_r, \beta, \beta') = -\frac{1}{2\beta}\left\{-\frac{\beta^2}{2}(q^p + \epsilon^2 q^s) + \beta\beta' q_r^p + \frac{\beta^2}{2}(1+\epsilon^2)\right\} \tag{4.28}$$

To compute the internal energy under the deformation, one may simply consider $e = \frac{\partial}{\partial\beta}(\beta V_{FP})$, as this gives the thermal average of the energy of the constrained replica subsequently averaged over the reference configuration:

$$\frac{\partial}{\partial\beta}(\beta V_{FP}) = \frac{1}{N}\overline{\left\langle \frac{\int \mathrm{D}\sigma^{(2)} H_\epsilon[\sigma^{(2)}] \exp\left(-\beta H_\epsilon[\sigma^{(2)}]\right)\delta\left(q_r - q_{\sigma^{(1)},\sigma^{(2)}}\right)}{Z_\epsilon(\sigma^{(1)}, q_r)} \right\rangle}^{(J_p, \widetilde{J}_s)} \tag{4.29}$$

Taking this derivative, one finds

$$e = -\frac{1}{2}\left\{\beta(1+\epsilon^2) + \beta' q_r^p - \beta(q^p + \epsilon^2 q^s)\right\} \tag{4.30}$$

Here we do not vary the temperature of the state we are following , which is always equal to the temperature of the equilibrium glass, so $\beta = \beta'$ and one can write:

$$e = -\frac{1}{2}\left\{\beta(1+\epsilon^2) + \beta q_r^p - \beta(q^p + \epsilon^2 q^s)\right\} \tag{4.31}$$

We can check that at $\epsilon = 0$, $q = q_r = q_g$, one simply recovers the paramagnetic energy e_{para}:

$$e|_{\epsilon=0} = -\frac{1}{2}\left(\beta + \beta q_g - \beta q_g\right) = -\frac{\beta}{2} = e_{para} \tag{4.32}$$

[3] q is to be determined at the saddle point.

4.4 Replica symmetry breaking

We now consider again the action S, equation (4.17), in the limit $m \to 0$:

$$S(Q,P,R) = \frac{\beta^2}{4}\left[\sum_{\alpha,\beta=1}^{n} R^p_{\alpha\beta} + 2nq_r^p + \epsilon^2 \sum_{\alpha\beta=1}^{n} R^s_{\alpha\beta}\right] + \frac{1}{2}\ln\det \mathbf{Q} \tag{4.33}$$

The determinant of $\mathbf{Q}$ can be split into two contributions, where the first vanishes and the second is $\det(\tilde{R})$, where $\tilde{R}$ is defined as:

$$\tilde{R} = R - q_r q_r^T \tag{4.34}$$

If we then consider full replica symmetry breaking ansatz, the matrix $\tilde{R}$ will be a Parisi matrix parametrized by $\{1-q_r^2, q(x)-q_r^2\}$. The entropic term in the action, i.e. the one coming from the determinant, can be computed using the general formula [20]:

$$\lim_{n\to 0}\partial_n\left[\frac{1}{2}\ln\det\tilde{R}\right] = \frac{1}{2}\left(\ln\left(1-\langle q\rangle\right) + \frac{q(0)-q_r^2}{(1-\langle q\rangle)} - \int_0^1 \mathrm{d}y \frac{1}{y^2}\ln\left(\frac{\lambda(y)}{(1-\langle q\rangle)}\right)\right) \tag{4.35}$$

where the average $\langle\cdot\rangle$ denotes the integral over the $[0,1]$ domain:

$$\langle\cdot\rangle = \int_0^1 \mathrm{d}x \quad . \tag{4.36}$$

and $\lambda(y)$ is given by:

$$\lambda(y) = 1 - xq(y) - \int_y^1 \mathrm{d}z q(z) \tag{4.37}$$

On the other hand, the energy term is given by the sum of the elements of the Hadamard power of matrix R. Because of the algebra of Parisi matrices, the p-th Hadamard power is also a Parisi matrix parametrized by $\{1, q(x)^p\}$. In terms of the set of parameters $\{m, q\}$, the full expression for discrete k is:

$$\begin{aligned}\sum_{\alpha\beta=1}^{n} R^p_{\alpha\beta} &= n\sum_{\beta=1}^{n} R^p_{1\beta} \\ &= n\left[1 + q_k^p(m_k-1) + q_{k-1}^p(m_{k-1}-m_k) + \cdots + q_0^p(n-m_0)\right]\end{aligned} \tag{4.38}$$

Once we take the continous limit ($k \to \infty$), we replace the differences $m_{i-1} - m_i$ by differentials $-\mathrm{d}x$, and thus the previous sum becomes an integral:

$$\sum_{\alpha\beta=1}^{n} R_{\alpha\beta}^{p} = n\left[1 - \int_{n}^{1} \mathrm{d}x q^{p}(x)\right] \simeq n\left[1 - \int_{0}^{1} \mathrm{d}x q^{p}(x)\right] \tag{4.39}$$

We have finally reached the expression for the action in the appropriate limit, which we will then have to extremize with respect to to the parameters $\{q(x), q_r\}$.

$$\begin{aligned}\lim_{n\to 0} \partial_n S\left[q(x), q_r\right] = \frac{\beta^2}{4}\left[\left(1 - \int_0^1 \mathrm{d}x q^p(x)\right) + 2q_r^p + \epsilon^2\left(1 - \int_0^1 \mathrm{d}x q^s(x)\right)\right] \\ + \frac{1}{2}\left[\ln\left(1 - \langle q\rangle\right) + \frac{q(0) - q_r^2}{(1 - \langle q\rangle)} - \int_0^1 \mathrm{d}y \frac{1}{y^2} \ln\left(\frac{\lambda(y)}{(1 - \langle q\rangle)}\right)\right]\end{aligned} \tag{4.40}$$

We firstly consider the extremum with respect to q_r, i.e.

$$\frac{d}{dq_r} \lim_{n\to 0} \partial_n S\left[q(x), q\right] = 0 \tag{4.41}$$

After some manipulations this derivative yields:

$$q_r = \frac{p\beta^2}{2} {q_r}^{p-1}(1 - \langle q\rangle) \tag{4.42}$$

which is consistent with the equation (4.23) we had obtained previously for q_r.

On the other hand, if we consider the variational derivative with respect to $q(x)$, that is

$$\frac{\delta}{\delta q(x)} \lim_{n\to 0} \partial_n S\left[q(x), q\right] = 0 \tag{4.43}$$

after some calculations we reach the equation:

$$\frac{q(0) - {q_r}^2}{(1 - \langle q\rangle)^2} + \int_0^x \mathrm{d}y \frac{\dot{q}(y)}{\lambda^2(y)} = \frac{\beta^2}{2}\left(pq^{p-1}(x) + \epsilon^2 s q^{s-1}(x)\right) \tag{4.44}$$

As a check of consistency, if in the previous equation we look for a replica symmetric solution ($q(x) = q$ constant) then we should recover the RS equation for q (4.25) . This is indeed the case.

Taking once the derivative of (4.44), we find

$$\frac{\dot{q}(x)}{\lambda^2(x)} = \frac{\beta^2}{2}\left[p(p-1)q^{p-2}(x) + \epsilon^2 s(s-1)q^{s-2}(x)\right]\dot{q}(x) \tag{4.45}$$

In the RS phase, this equation is fulfilled immediately as $\dot{q}(x) = 0$. Otherwise, the other term must vanish. In fact, the transition from one situation to the other is signalled by the replicon eigenvalue [21]:

$$\lambda_R = -1 + \frac{\beta^2}{2}\lambda^2(x)\left[p(p-1)q^{p-2}(x) + \epsilon^2 s(s-1)q^{s-2}(x)\right]\Big|_{q(x)=q^*} \tag{4.46}$$

If we increase the perturbation in the RS phase, at a certain point (ϵ,q), the eigenvalue may cross 0 (depending on the contol parameters and on p and s) and the RS solution may become unstable. [4]

If we now take another derivative in equation 4.44,we can find the breaking point x^*:

$$x^* = \frac{\lambda^3(x)\beta^2}{4}\left[p(p-1)(p-2)q^{p-3}(x) + \epsilon^2 s(s-1)(s-2)q^{s-3}(x)\right]\Big|_{q(x)=q^*} \tag{4.47}$$

Finally, taking one more derivative we can find the value of the derivative $\dot{q}(x^*)$ at the breaking point. One finds:

$$\dot{q}(x^*) = \frac{4}{\beta^2}\left[\lambda^3(x^*)g_2(x^*) - 3\lambda^2(x^*)x^* g_1(x^*)\right]^{-1} \tag{4.48}$$

where we have called $g_1(x)$ and $g_2(x)$ the functions:

$$g_1(x) = p(p-1)(p-2)q^{p-3}(x) + \epsilon^2 s(s-1)(s-2)q^{s-3}(x) \tag{4.49}$$

$$g_2(x) = p(p-1)(p-2)(p-3)q^{p-4} + \epsilon^2 s(s-1)(s-2)(s-3)q^{s-4}(x) \tag{4.50}$$

The function $\lambda(x)$ evaluated at the breaking point is just:

$$\lambda(x^*) = 1 - x^* q(x^*) - \int_{x^*}^{1} \mathrm{d}y q(y) = 1 - q^* \tag{4.51}$$

[4] In general, this replicon eigenvalue may be calculated directly from the stability matrix $M_{ab;cd} = \frac{\delta^2 S(Q)}{\delta Q_{ab}\delta Q_{cd}}\Big|_{Q=Q^*}$ evaluated at Q^*_{ab}, the RS saddle point solution. This eigenvalue λ_R is characterised by an eigenvector of the form $\delta_R Q_{ab} : \sum_{b(\neq a)} \delta_R Q_{ab} = 0 \quad \sum_{a(\neq b)} \delta_R Q_{ab}$, corresponding to a subspace of fluctuations called the *replicon subspace* [22].

4.5 Numerical solution of equations

4.5.1 Procedure and main results

Our procedure for studying glassy states is as follows. First we select a temperature T_g belonging to the interval $[T_K, T_d]$. We know that in this range of temperatures the phase space is composed of an exponential (in system size) number of metastable glassy states. Solving the polynomial equation (4.23):

$$q_g = \frac{\beta^2}{2} p {q_g}^{p-1}(1 - q_g) \tag{4.52}$$

we may compute the sef-overlap q_g of the undeformed glass prepared at temperature T_g. We thus select the secondary minimum of the Franz-Parisi potential (see section 2.3). Our *initial condition* is therefore $q_r = q = q_g$.

In terms of the analogy with structural glasses or hard spheres, lower values of T_g may be reached by slower and slower annnealing (when the system is finite-dimensional). Glasses prepared at lower values of T_g will be more and more stable, as reflected in a higher value of the self-overlap [5]. We will therefore consider glasses selected at different values of $T_g \in [T_K, T_d]$, and study their behaviour under deformmations of the form $H_{p+\epsilon s} = H_p[\sigma] + \epsilon H_s[\sigma]$. Depending on the value of T_g and the nature of the deformation s, we are presented with different scenarios. We will fix $p = 3$ in the following for simplicity.

The replica symmetric (RS) calculation tells us in all cases that the glass may be deformed up to a *yield value* (ϵ_Y), a spinodal point where the order parameter (the relative overlap q_r) jumps with a square root singularity. This spinodal point corresponds to the point where the glass yields. However, depending on the value of s, we find that before reaching the yield value the RS solution may become unstable, corresponding to the breaking of the original well-defined glass basin into sub-basins. This transition to an RSB phase witihin a glass is also called the *Gardner transition*. Depending on the slope of the overlap function at the breaking point, the glass basin may develop a 1-RSB structure or full-RSB structure. Thus the basin may break into disconnected clusters due to the adding of the s-spin constraints. Whether the behaviour predicted by the *unstable* RS computation will be altered when performing the full- (or k-) RSB calculation, i.e. whether the yielding transition in the broken phase will show the same behaviour, remains to be addressed.

[5] Regarding the height of the energy barrier to nucleation of the liquid phase, this is always infinite as we are in mean-field (fully-connected model).

4.5.2 Replica symmetric (elastic) yielding (s=2)

For low values of s, the replica symmetric calculation is stable all the way up to yielding. We may call this *elastic* yielding (there is no plastic regime before the material yields). Figure 4.1 shows q_r and q under the $s = 2$ deformation; they both disappear with a square root singularity at the spinodal point.

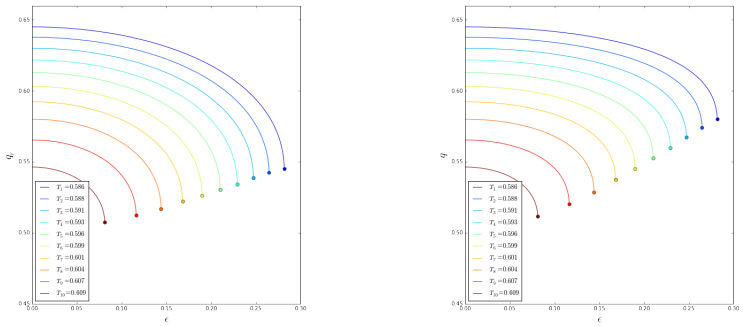

(a) Relative overlap with reference q_r, $s = 2$ deformation

(b) Internal overlap q, $s = 2$ deformation

Figure 4.1: Evolution of q_r and q for $p = 3$, $s = 2$

In the following figure 4.2 we see the evolution of the replicon eigenvalue λ_R. We see it stays negative all the way up to yielding, signaling that the RS phase is stable during the whole deformation.

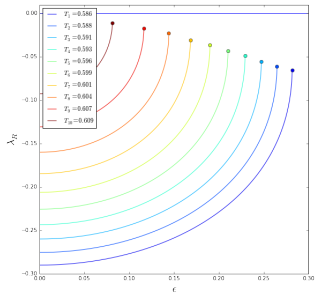

Figure 4.2: Replicon eigenvalue under $s = 2$ deformation. The RS phase is stable up to yielding

To gain insight into what is happening in the replica-symmetic regime, we may study how the internal energy is accumulated in the glass as the deformation is

increased. Following the analogy with structural glasses and real amorphous solids, we may think of the s-spin perturbation as the equivalent of a *strain*, which causes the accumulation of additional internal energy in the glass. In fact what we plot in figure 4.3 is not precisely equation (4.31). We remove the first term, which is due simply to the change in variance or stregnth of the couplings. When we do this we are isolating the increase in energy due to the deformation, as we are comparing the energy accumulated in the glass with respect to that which would appear in a paramagnet/fluid subject to the same deformation. We call this quantity e_{excess}, and it is simply equal to $\frac{\beta}{2}\left(q^p + \epsilon^2 q^s - q_r^p\right)$.

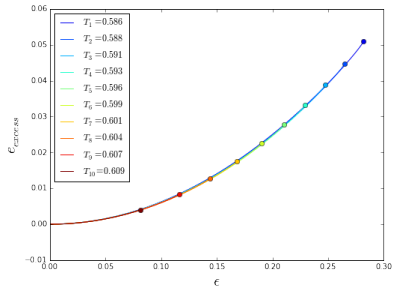

Figure 4.3: Excess energy of the glass under $s = 2$ deformation

We see that for all values of T_g, that is irrespectively of the degree of annealing, the glasses respond *elastically* to the deformation. They all follow the same approximately parabolic curve, and yield at different energies depending on the degree of annealing (glasses prepared at low T_g may be deformed further).

4.5.3 Limit case ($s = 3$)

We now consider the case $s = 3 = p$. In this case the random couplings constituting the deformation are of the same nature as the couplings of the orignal system. Thus an $s = 3$ deformation amounts to randomly perturbing the couplings, i.e. $J_{ijk} \to J_{ijk} + \epsilon \widetilde{J}_{ijk}$. This should *not* be confused with state following under cooling. Indeed if we decrease the temperature, we increase β and so it is equivalent to increasing the strength or variance of the couplings. However this is fundamentally different from randomly perturbing the couplings, in which case the variance is also increased, but the couplings are being *deformed* randomly at the same time. We should thus expect a glassy state which was at equilibrium in the original sample to become unstable at a critical value of the deformation. In figure 4.4, q and q_r are plotted. As in the previous case they display a spinodal point where they have a square root singularity.

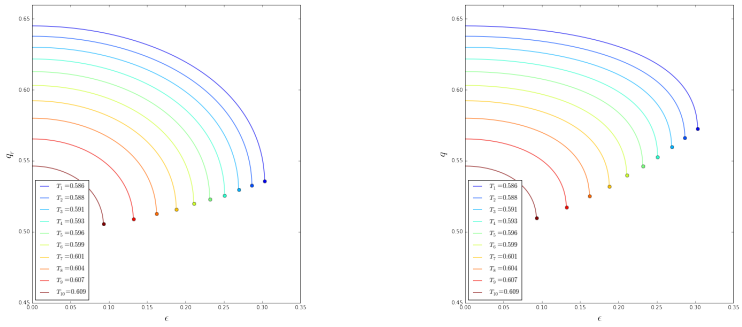

(a) Relative overlap with reference q_r, $s = 3$ deformation

(b) Internal overlap q, $s = 3$ deformation

Figure 4.4: Evolution of q_r and q for $p = 3$, $s = 3$

The deformation $s = 3$ is interesting because it turns out to be the upper limit of RS-stable yielding. As shown in figure 4.5, the replicon eigenvalue λ_R is 0 precisely at the yielding point. Although not shown here, this behaviour was also observed when studying the case $p = s = 4$. This points to a symmetry in the action S, which makes both the *longitudinal* and *replicon* modes coincide at the yielding point. However, we have not explored this point further and leave it for future research.

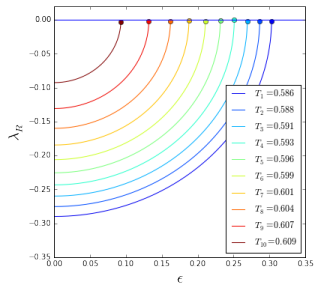

Figure 4.5: Replicon value under $s = 3 = p$ deformation. $\lambda_R = 0$ precisely at the yielding point ϵ_Y.

Finally, figure 4.6 shows the excess energy for $s = 3$. The system still behaves elastically, but the curves begin to separate, well-annealed glasses (lower T_g) having larger elastic moduli.

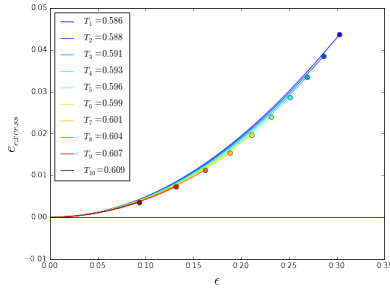

Figure 4.6: Excess energy of the glass under $s = 3$ deformation

4.5.4 RSB before yielding ($s > 3$)

We now explore larger values of s, ranging from 4 to 10. For these higher values of s we find that the RS phase becomes unstable prior to yielding. Figure 4.7 shows the typical behaviour of q_r and q (in particular what is shown is the case $s = 6$); the dashed line is the continuation of the RS solution in the unstable region. This now *unstable* RS solution continues to yield at a spinodal point, where the order parameters show again a square root singularity.

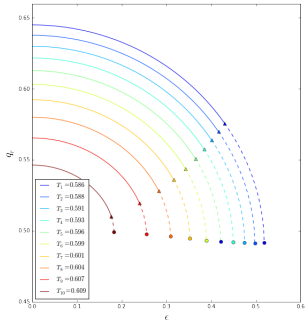

(a) Relative overlap with reference q_r, $s = 6$ deformation

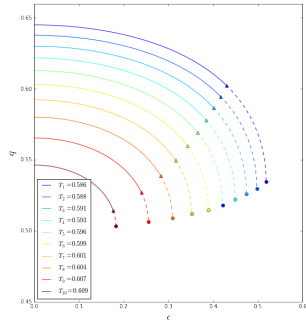

(b) Internal overlap q, $s = 6$ deformation

Figure 4.7: Evolution of q_r and q for $p = 3$, $s = 6$

We know the RS phase becomes unstable by studying the replicon eigenvalue λ_R as the glass is deformed (equation 5.65). This is shown in the following figure 4.8 (again for the case $s = 6$). We see that it becomes positive at a value of the perturbation which we call ϵ_G (Gardner transition).

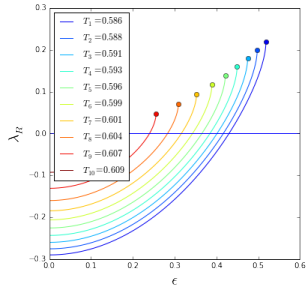

Figure 4.8: Replicon eigenvalue under $s = 6$ deformation

We now consider the excess energy of the glass under the deformation. The now *unstable* RS computation tells us that the energy overshoots, which is precisely what is observed also in the *shear stress* when following hard sphere glasses under strain [4]. The system first deforms in an elastic way, up to the Gardner transition (ϵ_G), where the deformation induces an RSB transition in the glass. Beyond this point one expects a *plastic* response characterized by soft modes and avalanches. In the full-RSB case, in particular, the system becomes *marginally stable*. We thus expect that in the RSB phase the response becomes *jerky*, and the system becomes unstable against collective rearrangements, as opposed to a simple elastic response.

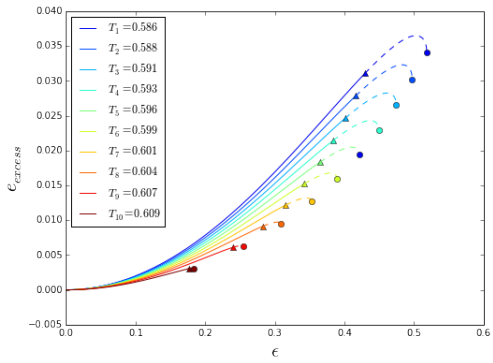

Figure 4.9: Excess energy of the glass under $s = 6$ deformation

In the different cases of s ranging from 4 to 10, one may use equation (5.70) to calculate the associated breaking point x^*. Figure 4.10 shows the different values of x^* obtained for various values of T_g and s. We find that for $T_g \to T_d$, x^* always tends to 0.5. The breaking point at the dynamical temperature T_d should be equal to the parameter exponent λ of the p-spin, which relates the dynamical exponents

a and b of the α and β regimes as one approaches T_d from above [6]. $x^* = 0.5$ is indeed the expected result for $p = 3$ [23]. In the other cases, the breaking point (via the associated parameter exponent λ), provides information on the critical slowing down of the dynamics within the glassy state close to the Gardner transition, where the glass splits into sub-basins with different associated relaxational timescales.

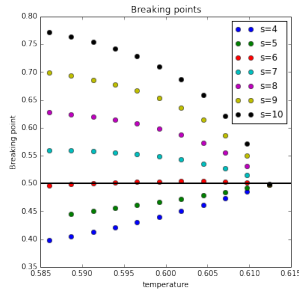

Figure 4.10: Breaking point x^* for increasing values of s. Near T_d, $x^* = 0.5$.

Finally, by studying the slope at the breaking point (equation 4.48), one may characterize the nature of the RSB transition. Indeed we know that a *positive* slope $\dot{q}(x^*) > 0$ signals a transition to full RSB. If instead it is negative, the flat plateau $q(x) = q_{RS} \quad \forall x$ develops a step (discontinuity), and the system is 1-RSB. The results are summarized in figure 4.11.

[6] The relation is the following: $\lambda = \frac{\Gamma^2(1-a)}{\Gamma(1-a)} = \frac{\Gamma^2(1+b)}{\Gamma(1+2b)}$, equal to 0.5 for the $p = 3$ spherical p-spin.

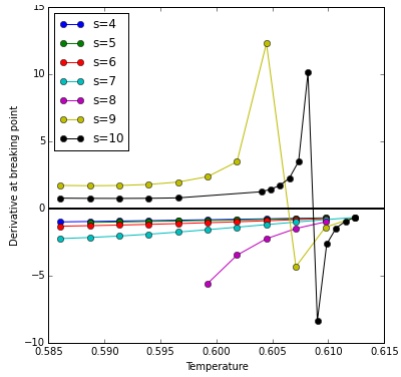

Figure 4.11: Slope at breaking point. As s is increased to 9,10, we find a Gardner transition to fullRSB (slope becomes positive).

For $s = 9, 10$, we see that a full RSB phase may appear as we deform the glass. Interestingly, this only occurs for glasses prepared at a temperature $T_g < T_*$ (figure 4.12). Thus for values of T_g too close to the dynamical temperature, the system doesn't develop a full RSB phase, at least at first. We do not know whether in the other cases there is a transition to full-RSB at some higher value of the deformation beyond the discrete replica symmetry breaking point.

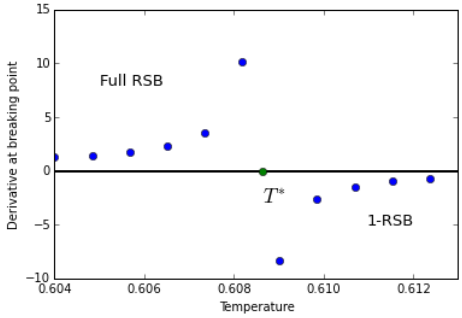

Figure 4.12: Plot of breaking point slope for $s = 10$ (near T_d), showing temperature $T_* < T_d$ below which there is a transition to full RSB.

To summarise, we have found that, having fixed $p = 3$ and varying the s-spin deformation, the glass may yield in different ways. For low values of s (<3), the yielding takes place within the initial purely elastic regime, and thus the system behaves in a regular manner up to the spinodal point. On the other hand, when higher ($s > 3$) values are considered, the deformation is capable of inducing an

RSB transition, thus signaling the transition from an *elastic* to a *plastic* regime, where the free energy landscape of the original glass basin which the system explores develops a complicated structure of sub-basins separated by barriers (of all scales in the full-RSB case). Thus although the RS calculation can be continued up to yielding, in this regime we expect an irregular behaviour characterized by avalanches and soft modes.

Chapter 5

Deforming Ising p-spin glassy states

We now turn to the case of the p-spin with discrete Ising variables. We may perform the same theoretical analysis as in the spherical case. Finally we report the result of Monte Carlo simulations of Ising spins on a fullly-connected lattice in order to test some of the analytical predictions.

5.1 Analytical approach

5.1.1 The replicated partition function

We now consider the p-spin Hamiltonian with Ising spins, that is:

$$H_p[\underline{\sigma}] = -\sum_{i_1<\cdots<i_p} J_{i_1\cdots i_p}\sigma_{i_1}\cdots\sigma_{i_p} \tag{5.1}$$

where the spins are now discrete Ising spins $\sigma_i = \pm 1$. The couplings are, as in the spherical case, Gaussian random variables with zero mean and variance:

$$\overline{J^2_{i_1\cdots i_p}} = \frac{p!}{2N^{p-1}} \tag{5.2}$$

In order to carry out the calculation of the Franz-Parisi potential, we introduce m *reference* replicas and n *constrained* replicas. We will want to consider the replicated partition function averaged over the quenched disorder:

$$\overline{Z_m \left\langle Z^n_\epsilon \right\rangle} \tag{5.3}$$

where the brackets denote the average over the reference replica. We will in the Ising case take a slightly different approach to the one taken in the previous section for the spherical model. In fact the two approaches are perfectly equivalent thanks to the simple structure of states in the p-spin model in the region $T \in [T_K, T_d]$ [1].

We introduce the same notation as in the spherical case (4.12), dividing the total overlap matrix $\underline{\underline{q}}$ into the sub-matrices Q (overlap of the reference replicas with themselves), P (relative overlap between reference and constrained replicas) and R (overlap of the constrained replicas with themselves). However, instead of considering the ansatz $Q = \delta_{ab}$, we will instead take the m reference replicas to be in the same state, i.e. $Q_{ab} = \delta_{ab} + (1 - \delta_{ab})q_g$ [2]. Correspondingly, the constrained replicas will have a fixed overlap q_r with respect to the reference ones, that is

$$\frac{1}{N}\underline{\sigma}^{a\in[1,m]} \cdot \underline{\sigma}^{b\in[m+1,m+n]} = q_r \tag{5.4}$$

and so instead of the ansatz $P_{a\alpha} = \delta_{a,1}q_r$ we take a matrix $P_{a\alpha} = q_r \quad \forall a, \alpha$. The matrix $\underline{\underline{q}}$ then takes the form:

$$\underline{\underline{q}} = \left[\begin{array}{ccc|ccc} 1 & \dots & q_g & q_r & \dots & q_r \\ \vdots & \ddots & \vdots & \vdots & \ddots & \vdots \\ q_g & \dots & 1 & q_r & \dots & q_r \\ \hline q_r & \dots & q_r & & & \\ \vdots & \ddots & \vdots & & R & \\ q_r & \dots & q_r & & & \end{array}\right] \tag{5.5}$$

To find the Franz-Parisi potential, we know that by construction:

$$\lim_{n\to 0} \partial_n \mathbb{E}_J \left[\log\left(Z_m \left\langle Z_\epsilon^n \right\rangle\right)\right]\Big|_{m\to 1} = -\beta V_{FP} \tag{5.6}$$

where brackets denote the average over the reference replica. To find the expectation value over the couplings, one can use once more the replica trick and write:

$$\lim_{n\to 0} \partial_n \mathbb{E}_J \left[\log\left(Z_m \left\langle Z_\epsilon^n \right\rangle\right)\right]\Big|_{m\to 1} = \lim_{n\to 0}\lim_{s\to 0} \partial_n \partial_s \mathbb{E}_J \left[\left(Z_m \left\langle Z_\epsilon^n \right\rangle\right)^s\right]\Big|_{m\to 1} \tag{5.7}$$

[1] In particular, the quenched and annealed free energy coincide in the interval $T \in [T_K, T_d]$.

[2] Because we subsequently take $m \to 1$, q_g will in the end be irrelevant.

One may then average over the couplings and express the summation over the spins in terms of the *replicated* overlap matrix $\underline{\underline{\hat{q}}}$, which is an $(s \times (m+n)) \times (s \times (m+n))$ block matrix (as an example $s = 3$ is shown):

$$\left(Z_m \left\langle Z_\epsilon^n \right\rangle \right)^s \propto \int \mathrm{d}\underline{\underline{\hat{q}}} \exp\left(N \hat{S}(\underline{\underline{\hat{q}}}) \right) \tag{5.8}$$

$$\underline{\underline{\hat{q}}} = \begin{bmatrix} \underline{\underline{q}} & 0 & 0 \\ 0 & \underline{\underline{q}} & 0 \\ 0 & 0 & \underline{\underline{q}} \end{bmatrix} \tag{5.9}$$

Fortunately, there is no need to consider this full replicated matrix, as the s blocks are completely uncorrelated (their mutual overlaps are 0) in the temperature region of interest $T \in [T_K, T_d]$. This means we can factorize the total action $\hat{S}(\underline{\underline{\hat{q}}})$ into the contribution from each single block, and finally find the Franz-Parisi potential taking the limits $n \to 0$ and $m \to 1$:

$$\begin{aligned} V_{FP} &= -\frac{1}{\beta N} \lim_{n\to 0} \lim_{s \to 0} \partial_n \partial_s \left(\int \mathrm{d}\underline{\underline{q}} \exp\left(N S(\underline{\underline{q}}) \right) \right)^s \Big|_{m \to 1} \\ &= -\frac{1}{\beta N} \lim_{n \to 0} \partial_n \int \mathrm{d}\underline{\underline{q}} \exp\left(N S(\underline{\underline{q}}) \right) \Big|_{m \to 1} \end{aligned} \tag{5.10}$$

To proceed with the calculation of $\overline{Z_m \left\langle Z_\epsilon^n \right\rangle}$, we introduce an integral representation of the Dirac function (neglecting pre-factors), integrating over a new auxililary matrix $\underline{\underline{\lambda}}$:

$$\begin{aligned} \delta(\underline{\sigma}^{(a)} \cdot \underline{\sigma}^{(b)} - N q_{ab}) &= \int \left(\prod_{a<b} \mathrm{d}\lambda_{ab} \right) \exp\left(\sum_{a<b} \lambda_{ab} (N q_{ab} - \underline{\sigma}^{(a)} \cdot \underline{\sigma}^{(b)}) \right) \\ &= \int \left(\prod_{a<b} \mathrm{d}\lambda_{ab} \right) \exp\left(\frac{1}{2} \sum_{a \neq b} \lambda_{ab} (N q_{ab} - \underline{\sigma}^{(a)} \cdot \underline{\sigma}^{(b)}) \right) \end{aligned} \tag{5.11}$$

this will constitute the entropic term in the final action S. As regards the interaction term, the calculation is done in the same way as in the spherical case, and gives the same contribution:

$$\overline{Z_m\left\langle Z_\epsilon^n\right\rangle} = \sum_{\{\underline{\sigma}^a\}} \int \mathrm{d}\underline{\underline{\lambda}} \int \mathrm{d}\underline{\underline{q}} \exp\left(\frac{N}{2}\sum_{a\neq b}\lambda_{ab}q_{ab} - \frac{1}{2}\sum_{a\neq b}\lambda_{ab}\underline{\sigma}^{(a)}\cdot\underline{\sigma}^{(b)}\right)$$
$$\exp\left(\frac{N\beta^2}{4}\left(\sum_{a,b\in[1,m]}Q_{ab}^p + \sum_{\alpha=1}^{n}\sum_{\beta=1}^{n}R_{\alpha\beta}^p + 2\sum_{a=1}^{m}\sum_{\alpha=1}^{n}P_{a\alpha}^p + \epsilon^2\sum_{\alpha=1}^{n}\sum_{\beta=1}^{n}R_{\alpha\beta}^s\right)\right) \tag{5.12}$$

It is straightforward to see that the sum $\sum_{\{\underline{\sigma}^a\}}$ over $n+m$ replica configurations can be factorized into a product of N sums over $n+m$ single Ising spins, that is:

$$\sum_{\{\underline{\sigma}^a\}}\exp\left(-\frac{1}{2}\sum_{a\neq b}\lambda_{ab}\underline{\sigma}^{(a)}\cdot\underline{\sigma}^{(b)}\right) = \exp\left(N\log\left(\sum_{\sigma^{(1)}\dots\sigma^{(n+m)}} e^{-\frac{1}{2}\sum_{a\neq b}\lambda_{ab}\sigma^{(a)}\cdot\sigma^{(b)}}\right)\right) \tag{5.13}$$

Finally, we have the following expression for the replicated partition function averaged over the disorder:

$$\overline{Z_m\left\langle Z_\epsilon^n\right\rangle} = \iint \mathrm{d}\underline{\underline{\lambda}}\mathrm{d}\underline{\underline{q}}\exp\left(NS(\underline{\underline{q}},\underline{\underline{\lambda}})\right) \tag{5.14}$$

Where the following action $S(\underline{\underline{q}},\underline{\underline{\lambda}})$ will have to be evaluated at the corresponding saddle point values for $\underline{\underline{\lambda}}$ and $\underline{\underline{q}}$ (the first term is obtained taking into account that the diagonal terms q_{aa} are equal to one):

$$S(\underline{\underline{q}},\underline{\underline{\lambda}}) = \frac{1}{2}\sum_{a,b=1}^{m+n}\lambda_{ab}q_{ab} + \frac{\beta^2}{4}\left(\sum_{a,b\in[1,m]}Q_{ab}^p + \sum_{\alpha=1}^{n}\sum_{\beta=1}^{n}R_{\alpha\beta}^p + 2\sum_{a=1}^{m}\sum_{\alpha=1}^{n}P_{a\alpha}^p\right.$$
$$\left.+\epsilon^2\sum_{\alpha=1}^{n}\sum_{\beta=1}^{n}R_{\alpha\beta}^s\right) + \log\left(\sum_{\sigma^{(1)}\dots\sigma^{(n+m)}}\exp\left[-\frac{1}{2}\sum_{a\neq b}\lambda_{ab}\sigma^{(a)}\cdot\sigma^{(b)}\right]\right) \tag{5.15}$$

5.1.2 Entropic term

The calculation will be carried out in the general full RSB setting, and then the replica symmetric equations will be extracted as a particular case. We will thus

consider the two matrices $\underline{\underline{q}}$ and $\underline{\underline{\lambda}}$ parametrized by

$$\underline{\underline{q}} = \left[\begin{array}{ccc|ccc} 1 & \dots & q_g & q_r & \dots & q_r \\ \vdots & \ddots & \vdots & \vdots & \ddots & \vdots \\ q_g & \dots & 1 & q_r & \dots & q_r \\ \hline q_r & \dots & q_r & 1 & \dots & q(x) \\ \vdots & \ddots & \vdots & \vdots & \ddots & \vdots \\ q_r & \dots & q_r & q(x) & \dots & 1 \end{array}\right] \quad \underline{\underline{\lambda}} = \left[\begin{array}{ccc|ccc} \lambda_0 & \dots & \lambda_g & \lambda_p & \dots & \lambda_p \\ \vdots & \ddots & \vdots & \vdots & \ddots & \vdots \\ \lambda_g & \dots & \lambda_0 & \lambda_p & \dots & \lambda_p \\ \hline \lambda_p & \dots & \lambda_p & \lambda_d & \dots & \lambda(x) \\ \vdots & \ddots & \vdots & \vdots & \ddots & \vdots \\ \lambda_p & \dots & \lambda_p & \lambda(x) & \dots & \lambda_d \end{array}\right] \tag{5.16}$$

In order to compute the entropic contribution, it is very useful to introduce the following identity [24][25]:

$$\begin{aligned} &\log\left(\sum_{\sigma^{(1)}\dots\sigma^{(n+m)}} \exp\left[-\frac{1}{2}\sum_{a\neq b}\lambda_{ab}\sigma^{(a)}\sigma^{(b)}\right]\right) \\ &= \log\left[\sum_{\sigma^{(1)}\dots\sigma^{(n+m)}} \exp\left(-\frac{1}{2}\sum_{a,b=1}^{m+n}\lambda_{ab}\frac{\partial^2}{\partial h_a \partial h_b}\right)\prod_{c=1}^{m+n}\exp\left(h_c\sigma_c\right)\Big|_{\underline{h}=0}\right] \\ &= \log\left[\exp\left(-\frac{1}{2}\sum_{a,b=1}^{m+n}\lambda_{ab}\frac{\partial^2}{\partial h_a \partial h_b}\right)\prod_{c=1}^{m+n}2\cosh\left(h_c\right)\Big|_{\underline{h}=0}\right] \end{aligned} \tag{5.17}$$

We can now take into account the parametrized structure of $\underline{\underline{\lambda}}$ and single out the various contributions to the differential operator:

$$\begin{aligned} &\exp\left(-\frac{1}{2}\sum_{a,b=1}^{m+n}\lambda_{ab}\frac{\partial^2}{\partial h_a \partial h_b}\right)\prod_{c=1}^{m+n}2\cosh\left(h_c\right)\Big|_{\underline{h}=0} = \\ &\exp\left[-\lambda_p\left(\sum_{a=1}^{m}\frac{\partial}{\partial h_a}\right)\left(\sum_{b=1}^{m+n}\frac{\partial}{\partial h_b}\right)\right]\underbrace{\exp\left[-\frac{1}{2}\sum_{a,b=1}^{m}\lambda_{ab}\frac{\partial^2}{\partial h_a \partial h_b}\right]\prod_{c=1}^{m}2\cosh\left(h_c\right)\Big|_{\underline{h}=0}}_{A} \\ &\underbrace{\exp\left[-\frac{1}{2}\sum_{a,b=m+1}^{m+n}\lambda_{ab}\frac{\partial^2}{\partial h_a \partial h_b}\right]\prod_{c=m+1}^{m+n}2\cosh\left(h_c\right)\Big|_{\underline{h}=0}}_{B} \end{aligned} \tag{5.18}$$

The first term A, which only involves the section corresponding to *reference* replicas, is straightforward to compute. To do this we introduce the following identity, which can be proven by considering the Taylor expansion:

$$\begin{aligned} \exp\left[\frac{\omega}{2}\frac{\partial^2}{\partial h^2}\right] f(h) &= \int_{-\infty}^{\infty} \frac{\mathrm{d}z}{\sqrt{2\pi\omega}} e^{\frac{-z^2}{(2\omega)}} f(h-z) \\ &\equiv \gamma_\omega \star f(h) \end{aligned} \tag{5.19}$$

Using this property we can write:

$$\begin{aligned} A &= \exp\left[-\frac{\lambda_g}{2}\left(\sum_{a=1}^{m}\frac{\partial}{\partial h_a}\right)^2\right]\left[\prod_{c=1}^{m} e^{-\frac{1}{2}(\lambda_0-\lambda_g)\frac{\partial^2}{\partial h_c^2}} 2\cosh(h_c)\Big|_{\underline{h}=0}\right] \\ &= \exp\left[-\frac{\lambda_g}{2}\left(\sum_{a=1}^{m}\frac{\partial}{\partial h_a}\right)^2\right]\prod_{c=1}^{m} g_g(1,h_c)\Big|_{\underline{h}=0} \end{aligned} \tag{5.20}$$

where, for reasons that will become clear in the following section, we have defined the function:

$$g_g(1,h_c) = \gamma_{-(\lambda_0-\lambda_g)} * 2\cosh(h_c) \tag{5.21}$$

At this point we introduce another identity. We have that:

$$\left(\sum_{a=1}^{n}\frac{\partial}{\partial h}\right)^k R(h_1,\ldots,h_k) = \frac{\partial^k}{\partial h^k} R(h,\ldots,h) \quad \forall k \tag{5.22}$$

In particular, applying this identity for $k=1$, we can write

$$\mathrm{A} = \exp\left[-\frac{\lambda_g}{2}\frac{\partial^2}{\partial\left(h^{(1)}\right)^2}\right] g^m(1,h^{(1)})\Big|_{h^{(1)}=0} \tag{5.23}$$

Parisi flow equation [26]

We now turn to the calculation of the B term in equation 5.18, which involves the *constrained* replicas and thus the full RSB part of the matrix $\underline{\underline{\lambda}}$:

$$\mathrm{B} = \exp\left[-\frac{1}{2}\sum_{a,b=1}^{m+n}\lambda_{ab}\frac{\partial^2}{\partial h_a \partial h_b}\right]\left(\prod_{c=m+1}^{m+n} 2\cosh(h_c)\right) \tag{5.24}$$

This is indeed more complicated, but we can exploit the block-structure of the matrix (figure 5.1) and iterate the procedure we used for calculating the previous term A.

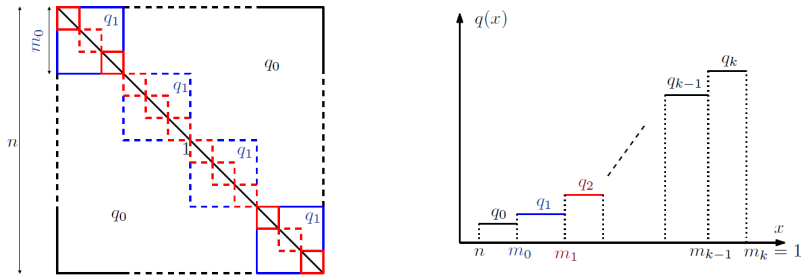

(a) Block structure of matrix

(b) k-RSB

Figure 5.1: Block structure and values q_k and m_k in the k-RSB ansatz.

We start from the innermost (diagonal) element of the matrix $\underline{\underline{\lambda}}$ and proceed outwards. Therefore, calling λ_d the diagonal element and λ_k the value in the innermost block, we have the following *initial condition* for $g(x, h)$:

$$\begin{aligned} g(1,h) &= g(m_k,h) \\ &= \exp\left[-\frac{1}{2}\left(\lambda_d-\lambda_k\right)\frac{\partial^2}{\partial h^2}\right]\left(2\cosh\left(h_c\right)\right) \\ &= \gamma_{-(\lambda_d-\lambda_k)} \star \left(2\cosh\left(h_c\right)\right) \end{aligned} \tag{5.25}$$

We then apply the next term corresponding to $\{q_{k-1}, m_{k-1}\}$ and define $g(m_{k-1}, h)$ as:

$$g(m_{k-1},h) = \exp\left[-\frac{1}{2}\left(\lambda_k-\lambda_{k-1}\right)\frac{\partial^2}{\partial h^2}\right] g^{m_{k-1}}(1,h) \tag{5.26}$$

We can then iterate this procedure in order to find a differential equation for $g(x, h)$. We have in general that:

$$g(m_i,h) = \exp\left[-\frac{1}{2}\left(\lambda_{i+1}-\lambda_i\right)\frac{\partial^2}{\partial h^2}\right] g^{\frac{m_i}{m_{i+1}}}(m_{i+1},h) \tag{5.27}$$

We now go to the full RSB continous limit, where we can write:

$$m_{i+1} = m_i + dx \qquad \lambda_{i+1} - \lambda_i = \dot{\lambda}(x) \tag{5.28}$$

substituting this into (5.27), we obtain the equation:

$$\begin{aligned} g(x,h) &= \exp\left[-\frac{\dot\lambda(x)}{2}dx\frac{\partial^2}{\partial h^2}\right] g^{\frac{x}{x+dx}}(x+dx,h) \\ &\sim \left[1-\frac{\dot\lambda(x)}{2}dx\frac{\partial^2}{\partial h^2}\right]\left[\exp\left(\left(1-\frac{dx}{x}\right)\log\big(g(x+dx,h)\big)\right)\right] \\ &\sim \left[1-\frac{\dot\lambda(x)}{2}dx\frac{\partial^2}{\partial h^2}\right]\left[g(x,h)\left(1-\frac{dx}{x}\log g(x,h)+dx\frac{\partial}{\partial x}\log g(x,h)\right)\right] \\ &\sim g(x,h)-\frac{\dot\lambda(x)}{2}dx\frac{\partial^2}{\partial h^2}g-\frac{dx}{x}g\log g+dxg\frac{\partial}{\partial x}\log g \end{aligned} \tag{5.29}$$

We thus have the following differential equation for $g(x,h)$:

$$g\frac{\partial}{\partial x}\log g=\frac{\dot\lambda(x)}{2}\frac{\partial^2 g}{\partial h^2}+\frac{1}{x}g\log g \tag{5.30}$$

It will be simpler to define the following function

$$f(x,h)=\frac{1}{x}\log\big(g(x,h)\big)\qquad g(x,h)=\exp\big(xf(x,h)\big) \tag{5.31}$$

In terms of which the differential equation (5.30) becomes:

$$\frac{\partial f}{\partial x}=\frac{\dot\lambda(x)}{2}\left[\frac{\partial^2 f}{\partial h^2}+x\left(\frac{\partial f}{\partial h}\right)^2\right] \tag{5.32}$$

This is the *Parisi flow equation* [26], which was first obtained in the context of the Sherrington-Kirkpatrick model. The initial condition for $f(x,h)$, on the other hand, is now:

$$f(1,h)=\log\big(g(1,h)\big)=\log\Big(\gamma_{-(\lambda_d-\lambda(1))}\star 2\cosh h\Big) \tag{5.33}$$

We can write finally the expression for B, in terms of the last convolution (corresponding to n, m_0). We also have to bear in mind that in the full RSB scheme $m_0\to n\to 0$:

$$\mathrm{B}=\gamma_{-\lambda(0)}*\exp\left[\frac{n}{m_0}m_0 f(m_0,h)\right]=\gamma_{-\lambda(0)}*\exp\big[nf(n,h)\big] \tag{5.34}$$

Now that we have A and B, we can go back to the full equation (5.18) and replace them by our new expressions:

$$\exp\left(-\frac{1}{2}\sum_{a,b=1}^{m+n}\lambda_{ab}\frac{\partial^2}{\partial h_a \partial h_b}\right)\prod_{c=1}^{m+n}2\cosh\left(h_c\right)\Big|_{\underline{h}=0} \tag{5.35}$$
$$=\exp\left[-\frac{\lambda_g}{2}\frac{\partial^2}{\partial\left(h^{(1)}\right)^2}-\frac{\lambda(0)}{2}\frac{\partial^2}{\partial\left(h^{(2)}\right)^2}-\lambda_p\frac{\partial^2}{\partial h^{(1)}\partial h^{(2)}}\right]g_g^m(1,h^{(1)})\exp\left(nf(n,h^{(2)})\right)\Big|_{\underline{h}=0}$$

It will be convenient to introduce a two by two matrix $\underline{\underline{\Lambda}}$ defined as:

$$\underline{\underline{\Lambda}}=\begin{bmatrix}-\lambda_g & -\lambda_p\\ -\lambda_p & -\lambda(0)\end{bmatrix} \tag{5.36}$$

We can then write equation 5.35 as:

$$\exp\left[\frac{1}{2}\sum_{i,j=1}^{2}\Lambda_{ij}\frac{\partial^2}{\partial h^{(i)}\partial h^{(j)}}\right]g_g^m(1,h^{(1)})\exp\left(nf(n,h^{(2)})\right)\Big|_{h^{(1)}=h^{(2)}=0} \tag{5.37}$$

In order to compute the Franz-Parisi potential we will be interested in the limit of *constrained* replicas going to zero, i.e. $n\to 0$. We can thus expand the last exponential, and we get

$$\begin{aligned}&\exp\left[\frac{1}{2}\sum_{i,j=1}^{2}\Lambda_{ij}\frac{\partial^2}{\partial h^{(i)}\partial h^{(j)}}\right]g_g^m(1,h^{(1)})\exp\left(nf(n,h^{(2)})\right)\\ &\sim\exp\left[\frac{1}{2}\sum_{i,j=1}^{2}\Lambda_{ij}\frac{\partial^2}{\partial h^{(i)}\partial h^{(j)}}\right]g_g^m(1,h^{(1)})\left(1+nf(0,h^{(2)})\right)\Big|_{h^{(1)}=h^{(2)}=0}\end{aligned} \tag{5.38}$$

Noticing that in this sum of two terms the first one only depends on $h^{(1)}$, and is thus only affected by the first element of Λ_{ij}, we can write (5.38) as:

$$\begin{aligned}&\exp\left[-\frac{\lambda_g}{2}\frac{\partial^2}{\partial\left(h^{(1)}\right)^2}\right]g_g^m(1,h^{(1)})\Big|_{h^{(1)}=0}\\ &+n\exp\left[\frac{1}{2}\sum_{i,j=1}^{2}\Lambda_{ij}\frac{\partial^2}{\partial h^{(1)}\partial h^{(2)}}\right]f(0,h^{(2)})g_g^m(1,h^{(1)})\Big|_{h^{(1)}=h^{(2)}=0}\end{aligned} \tag{5.39}$$

We now need to take the logarithm of this expression in order to obtain the full entropic term in the action S (equation 5.15):

$$\log\left(\sum_{\sigma^{(1)}\dots\sigma^{(n+m)}}\exp\left[-\frac{1}{2}\sum_{a\neq b}\lambda_{ab}\sigma^{(a)}\sigma^{(b)}\right]\right)$$
$$=\log\left(\mathcal{N}\right)+\frac{n}{\mathcal{N}}\exp\left[\frac{1}{2}\sum_{i,j=1}^{2}\Lambda_{ij}\frac{\partial^2}{\partial h^{(1)}\partial h^{(2)}}\right]f(0,h^{(2)})g_g^m(1,h^{(1)})\Big|_{h^{(1)}=h^{(2)}=0} \tag{5.40}$$

where we have defined $\mathcal{N}$ as:

$$\mathcal{N}=\exp\left[-\frac{\lambda_g}{2}\frac{\partial^2}{\partial\left(h^{(1)}\right)^2}\right]g_g^m(1,h^{(1)})\Big|_{h^{(1)}=0} \tag{5.41}$$

Product term

We still have to consider the fist term in the action S (equation 5.15), which we can also write as a trace, that is:

$$\frac{1}{2}\sum_{a,b\,=1}^{m+n}\lambda_{ab}q_{ab}=\frac{1}{2}\mathrm{Tr}\left(\underline{\underline{q}}\,\underline{\underline{\lambda}}\right) \tag{5.42}$$

We take directly the case $m=1$. We thus have to find the trace of the product of two matrices of the form

$$\underline{\underline{q}}=\begin{bmatrix}1&\dots&q_r&\dots\\ \vdots&1&q(x)&\dots\\ q_r&q(x)&\ddots&q(x)\\ \vdots&q(x)&\dots&1\end{bmatrix}\quad\underline{\underline{\lambda}}=\begin{bmatrix}\lambda_0&\dots&\lambda_p&\dots\\ \vdots&\lambda_d&\lambda(x)&\dots\\ \lambda_p&\lambda(x)&\ddots&\lambda(x)\\ \vdots&\lambda(x)&\dots&\lambda_d\end{bmatrix} \tag{5.43}$$

We can decompose the trace into the part coming from the full RSB parts and the rest, that is:

$$\mathrm{Tr}\left(\underline{\underline{q}}\,\underline{\underline{\lambda}}\right)=\lambda_0+2nq_r\lambda_p+\mathrm{Tr}\left(DD'\right) \tag{5.44}$$

where D and D' are two parisi matrices parametrized respectively by $\{1,q(x)\}$ and $\{\lambda_d,\lambda(x)\}$. It is easy to see, taking first the k-RSB limit and then considering the continous limit, that:

$$\mathrm{Tr}\left(DD'\right)=n\left[\lambda_d-\int_0^1\mathrm{d}x q(x)\lambda(x)\right] \tag{5.45}$$

5.1.3 Saddle point equations

We can now write the full expression for the action S, for $m = 1$ and linear order in n. However, we will add two new terms to equation (5.15), in order to enforce the differential equation and the initial condition for $f(x, h)$, which are:

$$\begin{cases} \frac{\partial f}{\partial x} = \frac{\dot{\lambda}(x)}{2}\left[\frac{\partial^2 f}{\partial h^2} + x\left(\frac{\partial f}{\partial h}\right)^2\right] \\ f(1,h) = \log\left(\gamma_{-(\lambda_d - \lambda(1))} * 2\cosh h\right) \end{cases}$$

We will thus introduce the function $P(x, h)$ which will act as a Lagrange multiplier. We will choose it to be normalized, i.e. $\int_{-\infty}^{\infty} \mathrm{d}h P(x, h) = 1$. Our action will then be (at $m = 1$, linear order in n):

$$\begin{aligned} S\left[\underline{\underline{q}}, \underline{\underline{\lambda}}; P(x,h), f(x,h)\right] = \\ \frac{1}{2}\lambda_0 + \frac{n}{2}\left[2q_r\lambda_p + \lambda_d - \int_0^1 \mathrm{d}x q(x)\lambda(x)\right] + \log\left(\mathcal{N}\right) + \frac{\beta^2}{4} \\ + \frac{\beta^2}{4} n\left[2q_r^p + \left(1 - \int_0^1 \mathrm{d}x q^p(x)\right) + \epsilon^2\left(1 - \int_0^1 \mathrm{d}x q^s(x)\right)\right] \\ + \frac{n}{\mathcal{N}}\exp\left[\frac{1}{2}\sum_{i,j=1}^{2}\Lambda_{ij}\frac{\partial^2}{\partial h^{(1)}\partial h^{(2)}}\right] f(0, h^{(2)}) g_g(1, h^{(1)})\Big|_{h^{(1)}=h^{(2)}=0} \\ + n\int_0^1 \mathrm{d}x \int_{-\infty}^{\infty} \mathrm{d}h P(x,h)\left[\frac{\partial f}{\partial x} - \frac{\dot{\lambda}(x)}{2}\left[\frac{\partial^2 f}{\partial h^2} + x\left(\frac{\partial f}{\partial h}\right)^2\right]\right] \\ + n\int_{-\infty}^{\infty} \mathrm{d}h P(1,h)\left[f(1,h) - \log\left(\gamma_{-(\lambda_d - \lambda(1))} * 2\cosh h\right)\right] \end{aligned} \tag{5.46}$$

We will now proceed to finding the saddle point equations involving q_r, $q(x)$, λ_p, $\lambda(x)$, $P(x, h)$ and $f(x, h)$ [27]. The other parameters won't contribute to the extremisation of the Franz Parisi potential.

- q_r

  The extremisation with respect to q_r gives

$$\lambda_p = -\frac{\beta^2}{2} p q_r^{p-1} \tag{5.47}$$

- $q(x)$

  Extremisation with respect to $q(x)$ yields

$$\lambda(x) = -\frac{\beta^2}{2}\left(pq^{p-1}(x) + \epsilon^2 sq^{s-1}(x)\right) \tag{5.48}$$

- $P(x,h)$, $P(1,h)$

  Extremising with respect to the Lagrange multipliers just gives back

$$\begin{cases} \frac{\partial f}{\partial x} = \frac{\dot{\lambda}(x)}{2}\left[\frac{\partial^2 f}{\partial h^2} + x\left(\frac{\partial f}{\partial h}\right)^2\right] \\ f(1,h) = \log\left(\gamma_{-(\lambda_d - \lambda(1))} \star 2\cosh h\right) \end{cases}$$

- $f(0,h)$

  The functional derivative with respect to $f(0,h)$ affects the two following terms:

$$\frac{\delta}{\delta f(0,h)}\left(\frac{1}{\mathcal{N}}\exp\left[\frac{1}{2}\sum_{i,j=1}^{2}\Lambda_{ij}\frac{\partial^2}{\partial h^{(1)}\partial h^{(2)}}\right] f(0,h^{(2)})g_g(1,h^{(1)})\Big|_{h^{(1)}=h^{(2)}=0}\right) + \frac{\delta}{\delta f(0,h)}\left(\int_0^1 \mathrm{d}x \int_{-\infty}^{\infty} \mathrm{d}h P(x,h)\frac{\partial f}{\partial x}\right) = 0 \tag{5.49}$$

  which are straightforward to carry out. Using again property (5.19), and introducing the pair of dummy variables $\underline{z} = \{z^{(1)}, z^{(2)}\}$, one finds:

$$P(0,h) = \frac{1}{\mathcal{N}}\int_{-\infty}^{\infty}\frac{\mathrm{d}z^{(1)}}{2\pi\sqrt{\det\Lambda}}\exp\left[-\frac{1}{2}\underline{z}^T\Lambda^{-1}\underline{z}\right] g_g(1,z^{(1)})\Big|_{z^{(2)}=h} \tag{5.50}$$

- $f(x,h)$

  The extremisation with respect to $f(x,h)$

$$\frac{\delta}{\delta f(x,h)}\int_0^1 \mathrm{d}x\int_{-\infty}^{\infty}\mathrm{d}h P(x,h)\left[\frac{\partial f}{\partial x} - \frac{\dot{\lambda}(x)}{2}\left[\frac{\partial^2 f}{\partial h^2} + x\left(\frac{\partial f}{\partial h}\right)^2\right]\right] \tag{5.51}$$
$$= 0$$

is carried out considering the integral by parts. To simplify the notation, we use the dot symbol for partial derivative with respect to x and the apostrophe $'$ for partial derivative with respect to h. One obtains the following partial differential equation for $P(x,h)$:

$$\dot{P}(x,h) = -\frac{\dot{\lambda}(x)}{2}\left[P''(x,h) - 2x(Pf')'\right] \tag{5.52}$$

- λ_p

  This derivative gives:

$$q_r = -\frac{\partial}{\partial\lambda_p}\left(\frac{1}{\mathcal{N}}\exp\left[\frac{1}{2}\sum_{i,j=1}^{2}\Lambda_{ij}\frac{\partial^2}{\partial h^{(1)}\partial h^{(2)}}\right] f(0,h^{(2)})g_g(1,h^{(1)})\Big|_{h^{(1)}=h^{(2)}=0}\right)$$
$$= -\frac{\partial}{\partial\lambda_p}\int_{-\infty}^{\infty}\mathrm{d}h P(0,h)f(0,h) \tag{5.53}$$

- $\lambda(x)$

  Considering extremization with respect to $\lambda(x)$, we get the following equation for the overlap function $q(x)$:

$$q(x) = \int_{-\infty}^{\infty}\mathrm{d}h P(x,h)\left(f'(x,h)\right)^2 \tag{5.54}$$

5.1.4 Replica symmetric equations

In the replica symmetric ansatz, the equations simplify as nothing depends on x. That is

$$\begin{cases} P(x,h) = P(0,h) \quad \forall x \\ f(x,h) = f(1,h) \quad \forall x \\ q(x) = q \quad \forall x \\ \lambda(x) = \lambda \quad \forall x \end{cases}$$

We thus have four equations to solve for four unknowns: λ, λ_p, q and q_r. The first two are straightforward:

$$\lambda_p = -\frac{\beta^2}{2} p q_r^{p-1} \quad \lambda = -\frac{\beta^2}{2}\left(p q^{p-1} + \epsilon^2 s q^{s-1}\right) \tag{5.55}$$

On the other hand, to write the equations for q and q_r we need to find the expression of the normalized distribution $P(0,h)$. Looking at equation (5.50) it may seem that there is also a dependence on λ_0, through $g_g(1,h)$, and on λ_g, present in Λ, but one finds that their contributions cancel out with the normalization. One finds:

$$P(0,h) = \frac{1}{\widetilde{\mathcal{N}}} \exp\left(\frac{h^2}{2\lambda}\right) \cosh\left(\frac{\lambda_p}{\lambda} h\right) \tag{5.56}$$

where $\widetilde{\mathcal{N}}$ is just a normalization factor:

$$\widetilde{\mathcal{N}} = \sqrt{2\pi(-\lambda)} \exp\left(-\frac{\lambda_p^2}{2\lambda}\right) \tag{5.57}$$

One can then proceed to write equation (5.54) for the overlap q. Again, although $f(1,h) = f(0,h)$ depends on λ_d, we are free to set $\lambda_d = \lambda$ as it only affects the normalization. Then $f(0,h)$ is given by $\log\left(2\cosh(h)\right)$, because it is just the convolution with a Gaussian of zero variance (a delta function). The equation for the overlap q is then:

$$q = \int_{-\infty}^{\infty} \mathrm{d}h P(0,h) \tanh^2(h) = \Big\langle \tanh^2(h) \Big\rangle_{\lambda,\lambda_p} \tag{5.58}$$

where we have introduced the notation $\langle\cdot\rangle = \int_0^1 \mathrm{d}x \int_{-\infty}^{\infty} \mathrm{d}h \cdot P(x,h)$.
Finally, to find the equation for q_r we need to consider the derivative:

$$\begin{aligned} q_r &= -\frac{\partial}{\partial \lambda_p} \int_{-\infty}^{\infty} \mathrm{d}h P(0,h) f(0,h) \\ &= -\frac{\partial}{\partial \lambda_p} \Big\langle \log\left(2\cosh(h)\right) \Big\rangle_{\lambda,\lambda_p} \end{aligned} \tag{5.59}$$

Taking the derivative and integrating by parts, one reaches the following equation for q_r:

$$q_r = \frac{1}{\widetilde{\mathcal{N}}} \int_{-\infty}^{\infty} \mathrm{d}h \exp\left(\frac{h^2}{2\lambda}\right) \sinh\left(\frac{\lambda_p}{\lambda}\right) \tanh(h) \tag{5.60}$$

Consistency check: in the unperturbed case ($\epsilon = 0$), we must have $q = q_r$, and thus equations (5.58) and (5.60) must be identical. Indeed, if $\lambda_p = \lambda$, we have:

$$\begin{aligned} q_r &= \frac{1}{\widetilde{\mathcal{N}}} \int_{-\infty}^{\infty} \mathrm{d}h \exp\left(\frac{h^2}{2\lambda}\right) \sinh(h) \tanh(h) \\ &= \frac{1}{\widetilde{\mathcal{N}}} \int_{-\infty}^{\infty} \mathrm{d}h \exp\left(\frac{h^2}{2\lambda}\right) \cosh(h) \tanh^2(h) \\ &= q \end{aligned} \tag{5.61}$$

5.1.5 Franz-Parisi potential

In order to find the replica-symmetric Franz-Parisi potential, all we need to do is consider the appropriate limit of the action S (equation 5.46), that is $V_{FP} = -\frac{1}{\beta} \lim_{n\to 0} \partial_n S(q_r.q)$. Bearing in mind that we have fixed $\lambda_d = \lambda$ in the normalization, one has:

$$\begin{aligned} V_{FP} = &-\frac{\beta}{4}(1+\epsilon^2) + \frac{\beta}{2}(p-1)q_r^p - \frac{\beta}{4}(p-1)q^p - \frac{\beta}{4}\epsilon^2(s-1)q^s \\ &+ \frac{\beta}{4}(pq^{p-1} + \epsilon^2 s q^{s-1}) - \frac{1}{\beta}\left\langle \log\left(2\cosh(h)\right)\right\rangle_{\lambda,\lambda_p} \end{aligned} \tag{5.62}$$

As a consistency check, one may evaluate the Franz-Parisi potential at $q = q_r = 0$, where one should recover the paramagnetic free energy. Indeed one finds:

$$V_{FP}(q = q_r = 0) = -\frac{\beta}{4} - \frac{1}{\beta}\left\langle \log\left(2\cosh(h)\right)\right\rangle_{\lambda,\lambda_p=0} = -\frac{\beta}{4} - \frac{1}{\beta}\log(2) = f_{para} \tag{5.63}$$

where $\log(2) = s_\infty$ is the entropy in the high-temperature limit.

In figure (5.2), $V_{FP} - f_{para}$ is plotted for overlaps $q_r \in [0.4, 0.9]$ at temperatures between T_K and T_d (0.651385 amd 0.681598 respectively). At each

value of q_r, the RS saddle point equations must first be solved to find q, and then the potential is evaluated. We find indeed that $V_{FP} - f_{para}$ at the secondary minimum (which is actually the complexity of the TAP states $\Sigma(f^*(T))$, see section 2.3) vanishes at T_K; and the minimum itself ceases to exist above T_d.

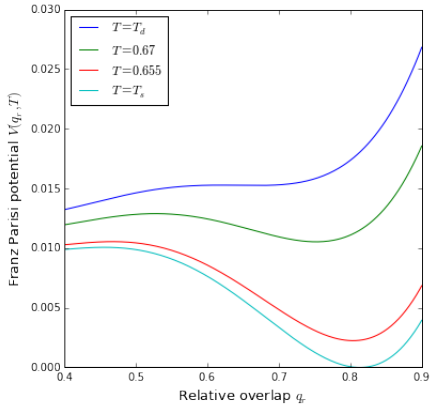

Figure 5.2: Franz-Parisi potential in the Ising case, in the interval $q_r \in [0.4, 0.9]$.

5.1.6 Replicon eigenvalue

We now turn to the caclulation of the replicon eigenvalue, and the breaking point where the RS phase becomes unstable. As in the case of the spherical p-spin, this is done by taking successive derivatives of the equation for the overlap function (5.54):

$$\dot{q}(x) = \frac{\mathrm{d}}{\mathrm{d}x} \int_{-\infty}^{\infty} \mathrm{d}h P(x,h) \left(f'(x,h)\right)^2 \tag{5.64}$$

In order to perform the derivatives, we will apply the flow equations:

$$\begin{cases} \dot{f} = \frac{\dot{\lambda}(x)}{2} \left[f'' + x \left(f'\right)^2 \right] \\ \dot{P}(x,h) = -\frac{\dot{\lambda}(x)}{2} \left[P''(x,h) - 2x(Pf')' \right] \end{cases}$$

We will not repeat here the full calculation, which involves several integrations by parts. One reaches:

$$\dot{q}(x)\left(-1+\frac{\beta^2}{2}\left[p(p-1)q^{p-2}(x)+\epsilon^2 s(s-1)q^{s-2}(x)\right]\left\langle \left(f''(x,h)\right)^2\right\rangle\right)=0 \tag{5.65}$$

The replicon eigenvalue, which signals the instability of the RS phase, is thus given by (coming from the RS phase):

$$\lambda_R=-1+\frac{\beta^2}{2}\left[p(p-1)q^{p-2}+\epsilon^2 s(s-1)q^{s-2}\right]\left\langle \left(f''(0,h)\right)^2\right\rangle \tag{5.66}$$

5.1.7 Breaking point

The breaking point is obtained by taking a further derivative of (5.65). At this point it is useful to define:

$$g_1=p(p-1)q^{p-2}+\epsilon^2 s(s-1)(s-2)q^{s-2} \tag{5.67}$$

$$g_2=p(p-1)(p-2)q^{p-3}+\epsilon^2 s(s-1)(s-2)q^{s-3} \tag{5.68}$$

$$g_3=p(p-1)(p-2)(p-3)q^{p-4}+\epsilon^2 s(s-1)(s-2)(s-3)q^{s-4} \tag{5.69}$$

After a somewhat lengthy calculation, one reaches the following expression for the breaking point:

$$x=\frac{g_2\langle(f'')^2\rangle+\frac{\beta^2}{2}g_1^2\langle(f''')^2\rangle}{\beta^2 g_1^2\langle(f'')^3\rangle} \tag{5.70}$$

Proceeding in a similar manner, one could also in principle compute the slope at the breaking point, as was done in the spherical case.

5.2 Numerical solution of equations

As was done in the spherical case, we may now solve the replica-symmetric saddle point equations as the deformation ϵ is increased. To do this, one needs to solve self-consistently, at each value of ϵ, the four equations for the four unknowns λ, λ_p, q and q_r. These are, respectively, equations (5.55), (5.60) and (5.58). On the other

hand, although we will not characterise the RSB phase, using equations (5.66) and (5.70) we may study the stability of the RS phase and compute the breaking point. Again we fix $p = 3$ for simplicity, and study different values of s.

In the following figure (5.3) we have plotted the case $s = 2$. q (solid lines) and q_r (dashed line) both jump with a square root singularity. On the other hand, the replicon eigenvalue tells us the RS phase is stable up to yielding, as in the spherical case. This $s = 2$ case will be the most interesting for the moment, as it is the deformation we will study using simulations in the final section (in particular we will consider the intermediate temperature $T = 0.67$).

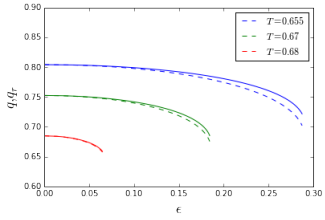

(a) Relative overlap (dashed line) and internal overlap (solid line) under $s = 2$ deformation.

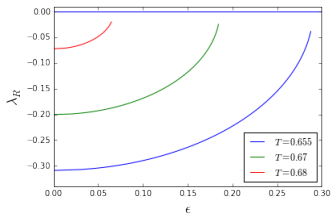

(b) Replicon eigenvalue under $s = 2$ deformation.

Figure 5.3: $s = 2$ is the only case where the RS phase is stable up to yielding.

For higher values of s (including for $s = 3$, unlike the spherical model), the replicon mode becomes unstable prior to yielding. The relative overlap is shown in figure 5.4. For simplicity we restrict the analysis to a single value of T_g, namely $T_g = 0.655$. s is then varied between 3 and 9. As before, the dashed lines represent the RS solution in the unstable regime.

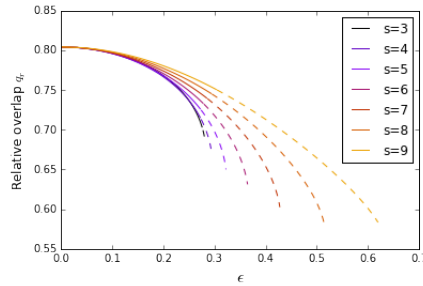

Figure 5.4: Deformation of $T_g = 0.655$ glass under increasing values of s. The dashed line is the RS-unstable regime.

In figure 5.5 we plot the replicon eigenvalue. It becomes unstable for all the values of $s \geq 3$ considered.

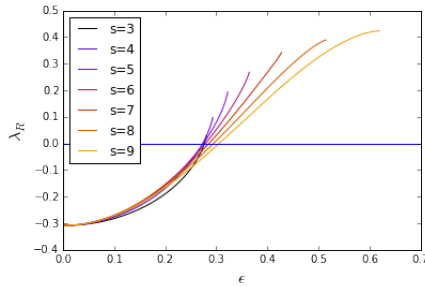

Figure 5.5: Replicon of the $T_g = 0.655$ glass along the deformation for increasing values of s. We see that it becomes unstable in all cases ($s \geq 3$).

Finally, we may make use of equation 5.70 to calculate the breaking point. As a check of consistency, we calculate it at $T_d = 0.68159$ and obtain $x^* = 0.7431$, which coincides with the values in [23] [3]. In table 5.1 we show the value of the breaking point as s is increased. The breaking point is at first below the T_d value, and then rises above as higher values of s are considered. The same thing was observed in the spherical case.

[3] As mentioned before in the spherical case, this is equal to the parameter exponent, which carries information on the critical slowing down at T_d.

Table 5.1: Breaking point (T_g=0.655)

s	ϵ	q_r	q	x^*
3	0.2756	0.7034	0.7327	0.6822
4	0.2720	0.7153	0.7328	0.6922
5	0.2738	0.7246	0.7405	0.7087
6	0.2774	0.7333	0.7476	0.7292
7	0.2846	0.7398	0.7529	0.7525
8	0.2932	0.7455	0.7575	0.7775
9	0.3049	0.7499	0.7611	0.8040

5.3 Monte Carlo simulations

In an attempt to test some of our predictions, we have carried out Monte Carlo simulations of spins on fully connected graphs. As we are interested in studying states below the dynamical temperature, we are presented with the problem of equilibration (the associated timescale diverges as $T \to T_d^+$. Luckily we can make use of the so-called *planting* technique [28], which essentially allows us to equilibrate for free in the glassy region $T \in [T_K, T_d]$.

5.3.1 Planting

To generate an instance $(\underline{\sigma}^*, G, J)$ of the planted spin glass one proceeds as follows:

- One first generates the *planted configuration* of spins σ_i^*, chosen uniformly at random between the 2^N possible configurations.

- One then generates a graph of interactions $G = (V, E)$; in our case we have only considered fully-connected graphs, but the planting method can be easily generalized to diluted models.

- For each triplet (i, j, k), the couplings J_{ijk} are chosen $+1$ or -1 according to:

$$P(J_{ijk}|\sigma_i^*, \sigma_j^*, \sigma_k^*) = \frac{\exp\left(\beta\frac{\sqrt{3}}{N}\sigma_i^*\sigma_j^*\sigma_k^*\right)}{2\cosh\left(\beta\frac{\sqrt{3}}{N}\right)} \tag{5.71}$$

  where due to the fully-connected nature of the interactions we have to bear in mind the proper scaling, which in the $p = 3$ case is precisely $J_{ijk} = \pm\sqrt{\frac{p!}{2N^{p-1}}} = \pm\frac{\sqrt{3}}{N}$.

If one considers the posterior distribution for the spins, it is easy to see that is it just given by the Boltzmann measure at inverse temperature β [28]:

$$P(\underline{\sigma}|J) = \frac{\prod_{i_1<\cdots<i_p} \exp\left(\beta J_{i_1\ldots i_p}\sqrt{\frac{p!}{2N^{p-1}}}\sigma_i\sigma_j\sigma_k\right)}{Z(\beta)} \tag{5.72}$$

The important property is that sampling from this posterior distribution will give an *equilibrium* configuration (in the context of [28] this corresponds to Bayes-optimal inference).

In figure 5.6 we show the value of the self-overlap of the equilibrium TAP states at temperatures between T_K and T_d, obtained by solving yhe replica symmetric equations (see subsection 5.1.4) at $\epsilon = 0$. A non-zero solution for the overlap first appears at T_d with a square root singularity, and increases as $T \to T_k^+$.

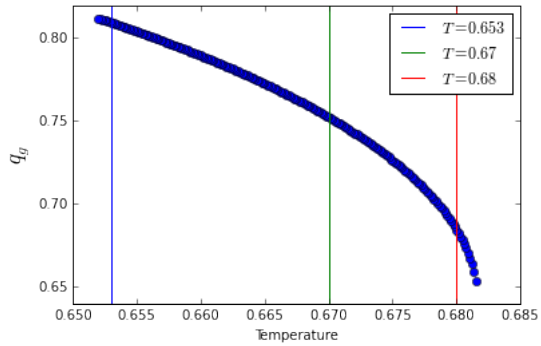

Figure 5.6: Self-overlap of the equilibrium glass states between T_K and T_d. The vertical lines are the temperatures where the simulations have been performed.

We now use planting to study the dynamics within one of these equilibrium glass states. We first generate a random initial configuration of spins $\underline{\sigma}(0)$; which will act as our *planted* configuration. We then generate the couplings (there will be $\frac{N(N-1)(N-2)}{3!}$ of them) following equation 5.71. Thus our initial random configuration is now an *equilibrium* configuration at temperature $T \in [T_K, T_d]$. Therefore if we run the Monte Carlo dynamics from the this initial planted configuration, the system should remain in the glass state for long times (the timescale diverges with system size). In particular, we may consider the correlation with the initial

configuration, given by:

$$C(t,0) = \frac{1}{N}\sum_{i=1}^{N}\sigma_i(t)\sigma_i(0) \tag{5.73}$$

If the initial configuration is an equilibrium one then this quantity should, after a short transient, descend to the corresponding value in figure 5.6. That is,

$$\lim_{t\to\infty}\frac{1}{N}\sum_{i=1}^{N}\sigma_i(t)\sigma_i(0) = q_g(T) \tag{5.74}$$

In figure 5.7, we show the results of the Montecarlo dynamics (starting from a planted configuration) at three different temperatures $T = 0.655$, 0.67 and 0.68.

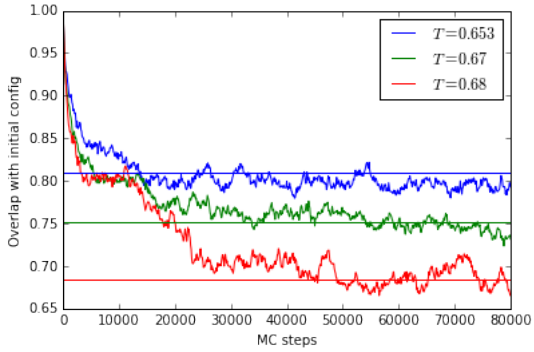

Figure 5.7: Montecarlo simulations using planting at the three temperatures. System size $N = 450$; averaged over 20 realizations at each temperature.

The simulations are computationally costly, because at each spin flip we must consider all the $O(N^3)$ triplets associated to the spin in question. We use $N = 450$, and there are strong finite-size effects so we average over 20 different runs. Despite the strong fluctuations, we see that the correlation decays rapidly to the value predicted by the RS equations at each temperature.

5.3.2 Adding the deformation

We may now finally consider the dynamics with the s-spin perturbation term. We proceed in the same manner as before, generating a planted configuration, but we now also create a symmetric matrix of pairwise couplings $\widetilde{J}_{ij}$, which will represent a conservative $s = 2$-spin deformation. We will thus be interesting in studying the evolution under the Hamiltonian:

$$H_3[\sigma] + \epsilon(t) H_2[\sigma] = -\sum_{i<j<k} J_{ijk}\sigma_i\sigma_j\sigma_k - \epsilon(t)\sum_{i<j}\widetilde{J}_{ij}\sigma_i\sigma_j \tag{5.75}$$

where the symmetric couplings $\widetilde{J}_{ij}$ are taken uniformly at random from a bimodal distribution with appropiate scaling $\widetilde{J}_{ij} = \pm\sqrt{\frac{s!}{2N}} = \pm\frac{1}{\sqrt{N}}$.

Starting from the equilibrium glass, we perform a sudden quench in the Hamiltonian ($\epsilon(t)$ is a stepwise function) and study the evolution using the Montecarlo update rule. The results are plotted in figure 5.8, where the temperature is $T = 0.67$. We consider 3 different values of ϵ. We first take $\epsilon = 0$, and we thus recover at long times $q_g(T = 0.67)$, the self-overlap of the equilibrium glass. If we increase ϵ a little amount to $\epsilon = 0.17 < \epsilon_Y$, we see that the overlap attained is slightly lower, and in fact corresponds fairly well to the value predicted by the RS equations (see figure 5.3a of the s=2 deformation). Finally, we consider a larger value of $\epsilon > \epsilon_Y$. In this case the system no longer remaines trapped near the planted configuration, and the overlap falls towards zero at long times. The Franz-Parisi potential tells us that the initial glass state has disappeared (become unstable); we do not know however what the final stationary state is (this is a purely dynamical question which we haven't addressed in this work).

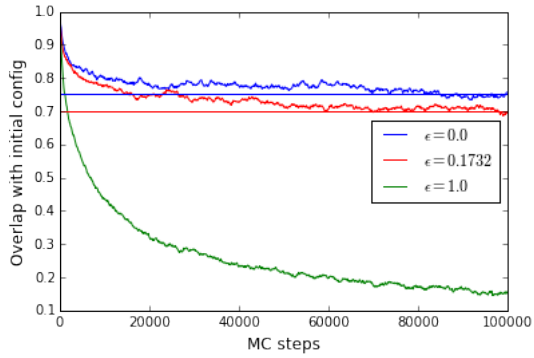

Figure 5.8: Correlation with initial configuration for $\epsilon = 0, 0.17, 1.0$. T=0.67. System size $N = 450$, averaged over 20 runs.

Although the general picture is recovered, the finite-size effects and long simulation times make it difficult to have a clear-cut view of the transition. A possible alternative would be to consider the dynamics on diluted graphs, where much larger system sizes can be attained.

Chapter 6

Conclusions and perspectives

In this final section we will review the main results obtained in this work, and briefly outline some perspectives for future research. In doing this it will be convenient to discuss separately the spherical case, where the equations are exactly solvable, and the Ising case, where the full-RSB equations are intractable but we can perform numerical simulations.

6.1 Spherical p-spin

By studying the Franz-Parisi potential of the deformed glass and the associated saddle point equations for the overlaps, we have found, depending on the values of p and s, a rich variety of behaviours approaching yielding. Fixing $p = 3$, at low values of s (<3), we find that the system is replica symmetric up to yielding. When s is increased to higher values, we find that the replicon eigenvalue becomes unstable along the deformation, and the glass undergoes a Gardner transition, yielding in a replica-symmetry broken phase.

Following the works of Crisanti and Leuzzi [18] [19], one may find the analytical solution in the full-RSB phase before yielding. As the model is analytically tractable, one may then characterise the fluctuations and associated susceptibilities at the yielding point in the different regimes.

The presence of quenched disorder in fact leads to two distinct susceptibilities. To study these susceptibilities, we need to distinguish all the different averages which have appeared during this work. Firstly, there is the *thermal* average of the constrained replica $\underline{\sigma}$, which is under the Hamiltonian $H_{p+\epsilon s}[\underline{\sigma}]$. We denote this average with brackets $\langle\cdot\rangle_{\text{th}}$, adding a subscript to distinguish it from the average

over the reference replica.

Secondly, we have the average over the reference configuration $\underline{\tau}$, which we denote again by brackets (without a subscript) $\langle\cdot\rangle$:

$$\langle\cdot\rangle = \int D\underline{\tau} \frac{1}{Z_J} \exp\left(-\beta H_p(\underline{\tau})\right)\cdot \tag{6.1}$$

Finally the overbar $\overline{\cdot}$ denotes as usual the average over the couplings $\int \mathrm{d}Jp(J)\cdot$. Considering all this notation, one may study the *connected* and *disconnected* suceptibilities [1]:

$$\chi_{con} = N\left(\overline{\langle\langle q_r^2\rangle_{\mathrm{th}}\rangle} - \overline{\langle\langle q_r\rangle_{\mathrm{th}}\rangle}^2\right) \tag{6.2}$$

$$\chi_{dis} = N\left(\overline{\langle\langle q_r\rangle_{\mathrm{th}}^2\rangle} - \overline{\langle\langle q_r\rangle_{\mathrm{th}}\rangle}^2\right) \tag{6.3}$$

The signature of random-field disorder is that $\chi_{dis} \propto \chi_{con}^2$, indicating that disorder-induced sample to sample fluctuations provide the dominant source of fluctuations [29]. It would be interesting to see whether the RFIM [30] behaviour is recovered in the present model, and what differences there are between the various RS/RSB regimes. This same question has been posed in the case of hard spheres and harmonic soft spheres [31][32], and we expect that in the p-spin the anlysis will be simpler to carry out, and may thus shed light on the nature of the yielding transition.

On the other hand, a complementary approach would be to study the dynamics of the model. The Langevin dynamics of the $p+\epsilon s$ model are given by:

$$\dot{\sigma}_i(t) = -\mu(t)\sigma_i(t) - \frac{\partial H_{p+\epsilon s}[\underline{\sigma}]}{\partial \sigma_i(t)} + \eta_i(t) \tag{6.4}$$

where $\eta_i(t)$ is a Gaussian white noise, with $\langle\eta_i(t)\rangle = 0$ and $\langle\eta_i(t)\eta_j(t')\rangle = 2T\delta_{ij}\delta\left(t-t'\right)$, and $\mu(t)$ is a Lagrange multiplier which is introduced in order to enforce the spherical constraint $\frac{1}{N}\sum_i^N \sigma_i^2(t) = 1$.

[1] In practice, this would involve introducing couplings between replicas and then sending these couplings to zero, as in section 2.3 where the Franz-Parisi potential was discussed as a Legendre transform.

In particular one would be interested in the dynamics starting from an initial configuration extracted at equilibrium from the unperturbed Hamiltonian, that is $p(\underline{\sigma}(0)) \sim \exp\big(-\beta H_p[\underline{\sigma}(0)]\big)$. From the dynamical equations it would be possible to explore further the behaviour in the marginally stable/RSB phase beyond the Gardner transition, where one expects the system to fall out of equilibrium and show aging effects (it can no longer explore freely the original glass basin, which becomes rough).

6.2 Ising p-spin

In the Ising case we have performed the same analysis of the Franz-Parisi potential of the glass under a deformation. We find, having again fixed $p = 3$, that for values of $s \geq 3$ the system undergoes an RSB instability before yielding. Although we can (and have) written down the full-RSB equations to find the breaking point, solving them analytically in the broken phase is difficult. In the Ising case it would therefore be interesting to pursue further numerical simulations. Indeed it would be interesting to study the distribution of avalanches near yielding, in the different RS and RSB regimes. One could also study the susceptibilities, considering sample-to-sample averages (that is, over the initial random configuration $\underline{\sigma}(0)$) and thermal averages over different runs with the same sample. All this would require having good enough statistics, which could be achieved by considering simulations on diluted (sparse) models (instead of fully connected graphs as done here).

Bibliography

[1] A. Cavagna, *Supercooled Liquids for Pedestrians*, Physics Reports 476, 51 (2009)

[2] G. Biroli and J. Bouchaud, in *Structural Glasses and Supercooled Liquids: Theory, Experiment and Applications*, edited by P.G.Wolynes and V.Lubchenko (Wiley and Sons, 2012), arXiv:0912.2542.

[3] Silvio Franz and Giorgio Parisi, *Recipes for metastable states in spin glasses* arXiv:cond-mat/9503167

[4] C. Rainone, P. Urbani, H. Yoshino, F. Zamponi, *Following the evolution of glassy states under external perturbations: compression and shear strain*, Phys. Rev. Lett. 114, 015701 (2015)

[5] Y. Sun, A. Crisanti, F. Krzakala, L. Leuzzi, L. Zdeborová *Following states in temperature in the spherical s+p-spin glass model*,J. Stat. Mech. (2012) P07002

[6] Daniel Bonn, Morton M Denn, Ludovic Berthier, Thibaut Divoux, and Sebastien Manneville, *Yield stress materials in soft condensed matter*,Reviews of Modern Physics 89, 035005 (2017).

[7] Y. Jin, P. Urbani, F. Zamponi, H. Yoshino *A stability-reversibility map unifies elasticity, plasticity, yielding and jamming in hard sphere glasses*, arXiv:1803.04597 [cond-mat.soft]

[8] Pierfrancesco Urbani and Francesco Zamponi, *Shear yielding and shear jamming of dense hard sphere glasses*, Physical review letters 118, 038001 (2017).

[9] B. Derrida, Phys. Rev. Lett. 45 79 (1980)

[10] D.J. Gross, M. Mezard, *The simplest spin glass*, Nuclear Physics B Volume 240, 1984

[11] A. Crisanti and H.-J. Sommers, Z. Phys. B 87, 341 (1992).

[12] DJ Thouless, PW Anderson and RG Palmer, Phil Mag 35 (1977) 593

[13] T. Castellani and A. Cavagna, *Spin glass theory for pedestrians*, arXiv:cond-mat/0505032 [cond-mat.dis-nn]

[14] Francesco Zamponi, *Mean field theory of spin glasses*, arXiv:1008.4844 [cond-mat.stat-mech]

[15] L. Berthier, J.L. Barrat and J. Kurchan, Phys. Rev. E 61, 5464 (2000).

[16] Ludovic Berthier, *Yield stress, heterogeneities and activated processes in soft glassy materials*, Journal of Physics: Condensed Matter, Volume 15, Number 11, 2003
[17] Francesco Zamponi, PhD thesis, arXiv:cond-mat/0510438 [cond-mat.dis-nn]
[18] A. Crisanti and L. Leuzzi, *Spherical 2+p spin-glass model: An analytically solvable model with a glass-to-glass transition*, Phys. Rev. B 73, 014412 (2006)
[19] A. Crisanti and L. Leuzzi, *Amorphous-amorphous transition and the two-step replica symmetry breaking phase*, Phys. Rev. B 76, 184417 (2007)
[20] Marc Mézard, Giorgio Parisi *Replica field theory for random manifolds*, Journal de Physique I, EDP Sciences, 1991, 1 (6), pp.809-836
[21] J. De Almeida and D. J. Thouless, *Stability of the Sherrington-Kirkpatrick solution of a spin glass model*, Journal of Physics A: Mathematical and General 11, 983 (1978).
[22] P. Urbani, *Statistical Physics of glassy systems: tools and applications*, IPhT lecture notes
[23] U. Ferrari, L. Leuzzi, G. Parisi, T. Rizzo *On the two-steps relaxation of mean field glasses: p-spin model*, Phys. Rev. B 86, 014204 (2012)
[24] H. Nishimori, *Statistical physics of spin glasses and information processing: an introduction*, vol. 111 (Clarendon Press, 2001).
[25] B. Duplantier, Journal of Physics A: Mathematical and General 14, 283 (1981).
[26] M. Mezard, G. Parisi, and M. A. Virasoro, *Spin glass theory and beyond* (World Scientific, Singapore, 1987).
[27] H -J Sommers and W Dupont, *Distribution of frozen fields in the mean-field theory of spin glasses*, Journal of Physics C: Solid State Physics, Volume 17, Number 32
[28] Lenka Zdeborová and Florent Krzakala, *Statistical physics of inference: thresholds and algorithms*, Advances in Physics Volume 65, 2016 - Issue 5
[29] M. Ozawa, L. Berthier, G. Biroli, A. Rosso, G. Tarjus, *A random critical point separates brittle and ductile yielding transitions in amorphous materials*, roc. Natl. Acad. Sci. USA 115, 6656 (2018)
[30] Nattermann T, *Theory of the random field ising model*, in Spin glasses and random fields (World Scientific), pp. 277-298 (1998)
[31] C. Rainone and P. Urbani, *Following the evolution of glassy states under external perturbations: the full replica symmetry breaking solution*, J. Stat. Mech. 053302 (2016)
[32] G.Biroli and P.Urbani, *Liu-Nagel phase diagrams in infinite dimension*, SciPost Phys. 4, 020 (2018)